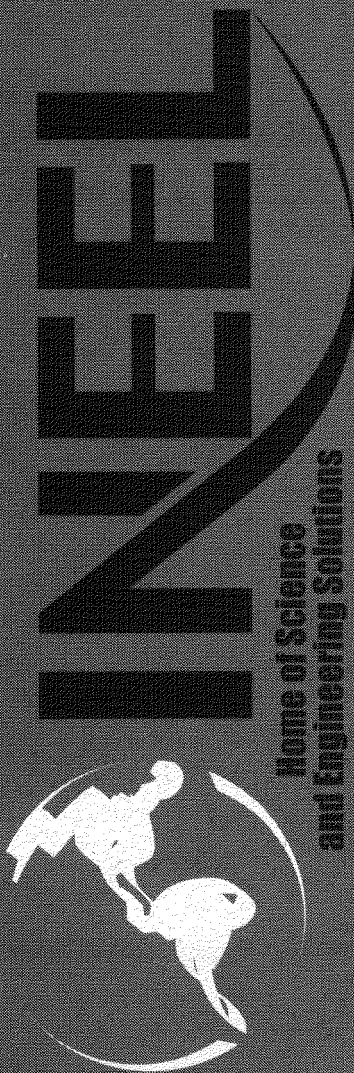


# ***Final Results Report, In Situ Grouting Technology for Application in Buried Transuranic Waste Sites***

*Volume 2*

*Evaluation of Proposed In Situ Grouting of  
Operable Unit 7-13/14 Waste against Limited  
Feasibility Study Criteria*

*Eric C. Miller  
Sheldon D. Smith  
June 2003*



*Idaho National Engineering and Environmental Laboratory  
Bechtel BWXT Idaho, LLC*

**Final Results Report,  
In Situ Grouting Technology for Application in Buried  
Transuranic Waste Sites**

***Volume 2***

**Evaluation of Proposed In Situ Grouting of  
Operable Unit 7-13/14 Waste against Limited  
Feasibility Study Criteria**

**Eric C. Miller  
Sheldon D. Smith**

**June 2003**

**Idaho National Engineering and Environmental Laboratory  
Idaho Completion Project  
Idaho Falls, Idaho 83415**

**Prepared for the  
U.S. Department of Energy  
Assistant Secretary for Environmental Management  
Under DOE Idaho Operations Office  
Contract DE-AC07-99ID13727**

## **ABSTRACT**

This document estimates the durability and evaluates the chemical buffering properties of a grouted waste form buried at the Subsurface Disposal Area at the Idaho National Engineering and Environmental Laboratory. Estimates of both durability and chemical buffering were made separately through theory and analytical solutions. In addition, numerical simulations were made to integrate these and other factors to produce mass release curves for each contaminant of potential concern. Numerical simulations were also performed to estimate the effects of freezing/thawing and seismic loading on a grouted waste monolith located at the Subsurface Disposal Area.



# CONTENTS

ABSTRACT.....	iii
ACRONYMS.....	ix
1. DURABILITY AND PERFORMANCE OF GROUTED WASTE MONOLITHS IN THE SUBSURFACE DISPOSAL AREA .....	1
1.1 Objective.....	1
1.1.1 Durability of Grouted Waste Monoliths.....	1
1.1.2 Monolith Cracking.....	5
1.2 Impacts of Freeze/Thaw and Seismic Activity on Grouted Monoliths in the Subsurface Disposal Area.....	5
2. CHEMICAL BUFFERING PROPERTIES OF THE GROUTED WASTE FORM.....	6
2.1 pH/Eh and Contaminants of Potential Concern Solubility in the Subsurface Disposal Area Subsurface.....	6
2.1.1 Pre-grout Ph/Eh in the Subsurface Disposal Area .....	6
2.1.2 Post-grout Eh/pH and Contaminants of Potential Concern Solubility in Subsurface Disposal Area Waste.....	8
2.2 Evaluation of the Chemical Buffering Properties of the Grouted Waste Form.....	8
3. SOURCE RELEASE MODELING .....	10
3.1 Modeling Objectives .....	10
3.2 Conceptual Model Development.....	10
3.2.1 Physical Characteristics of Materials .....	12
3.2.2 Pertinent Site Hydrology .....	12
3.2.3 Grouting Protocol .....	12
3.2.4 Contaminant Transport Mechanisms .....	13
3.3 Assumptions.....	14
3.3.1 Flow Modeling Assumptions .....	14
3.3.2 Transport Modeling Assumptions .....	14
3.4 Simulation Code.....	15
3.5 Discretization .....	16
3.6 Parameterization.....	18
3.7 Boundary Conditions.....	22

3.8	Initial Conditions.....	25
3.8.1	Solubility.....	27
3.8.2	Soilcrete Monolith Fracturing.....	28
3.8.3	Fracture Aperture.....	29
3.8.4	Baseline Fracture Density.....	29
3.8.5	Fracture Characterization.....	29
3.8.6	Contaminant of Potential Concern Mass Fraction Estimates.....	30
3.9	Base Case Results.....	35
3.9.1	Estimating Mass Release from the Grout Waste Monolith.....	35
3.9.2	Estimation of the Mass of Contaminants of Potential Concern Released from Monolith over 10,000 Years.....	36
3.10	Sensitivity Cases.....	40
3.10.1	Grid Discretization Density.....	40
3.10.2	Variability of Model Parameters.....	44
3.10.3	Sensitivity Case Analysis Summary.....	50
3.11	Modeling Limitations.....	52
3.11.1	Modeling Uncertainties.....	52
3.11.2	Modeling Limitations.....	52
4.	SUMMARY AND CONCLUSIONS.....	53
5.	REFERENCES.....	54
	Appendix A—Tabular and Graphical Mass Release Data for Contaminants of Potential Concern.....	57
	Appendix B—Estimation of Thermal Stresses in a Grouted Waste Monolith Under Freezing Conditions.....	83
	Appendix C—Estimation of Seismic Stresses in a Grouted Waste Monolith at the Radioactive Waste Management Complex.....	103

## FIGURES

1.	Characterization of waste buried at the Subsurface Disposal Area.....	11
2.	Matrix profile following grouting.....	13
3.	Matrix blocks in 3-D, and a 2-D representation of the nested grids within a matrix block.....	16
4.	Initial grid block geometry.....	17
5.	Grout waste monolith model design reduced scale.....	17
6.	X-Y plane view of column A11 1 and adjacent elements (U-V-W-X11 1) of layer 1.....	18
7.	Gas saturation distribution of the grout waste monolith model.....	22

8.	Cross section of the hydraulic flow patterns generated in the monolith. ....	23
9.	Horizontal flow values between the column and lateral elements. ....	24
10.	Horizontal flow values between lateral elements and side boundary. ....	24
11.	Vertical flow values of the column. ....	25
12.	Vertical flow values of lateral elements. ....	25
13.	Steady state saturation values for the monolith. ....	26
14.	Mass remaining curves of chemicals with no associative $K_d$ . ....	38
15.	Mass remaining curves of chemicals with increasing no associative $K_d$ . ....	39
16.	Mass remaining curves of U-238 and Pu-239. ....	39
17.	Mass remaining curve of Ac-227 and Am-241. ....	40
18.	Grid refinement (horizontal) and mass (Tc-99) remaining in monolith. ....	42
19.	Grid refinement (vertical) and mass (Tc-99) remaining in monolith. ....	43
20.	Mass released of GenRad because of variation in grout permeability. ....	45
21.	Mass release of GenRad with $K_d$ values of 0.0, 0.0005, 0.005 and 0.05 $m^3/kg$ during 3,000 years. ....	47
22.	Mass release of GenRad with $K_d$ values of 0.05, 0.5 and 1.0 $m^3/kg$ during 20,000 years. ....	47
23.	Mass release of GenRad with $K_d$ values of 1.0, 2.0, and 5.0 $m^3/kg$ during 20,000 years. ....	48
24.	Mass release of GenRad from nonfractured to fractured condition of the monolith. ....	50
25.	Mass release from monolith as the $K_d$ increases in magnitude in 100 years. ....	51

## TABLES

1.	Average leachability index results for each of the five neat grout tests. ....	2
2.	Leachability index for strontium for neat grout and neat grout with organics, nitrate salts, and soil for each of the five test grouts. ....	3
3.	Percent of original calcium remaining in neat grout at select times. ....	4
4.	Percent of original aluminum remaining in neat grout at select times. ....	4
5.	Percent of original silicon remaining in neat grout at select times. ....	4
6.	Estimated solubilities of Subsurface Disposal Area contaminants of potential concern at pH 7 and Eh of 800 mV. ....	7

7.	Estimated solubilities of grouted COPCs at pH 10.5 and Eh of 310 mV and –400 MV, and associated solubility change factors with respect to pre-grout conditions (Hull and Pace 2000). ....	9
8.	Contaminants of potential concern. ....	11
9.	Initial estimates of matrix parameters. ....	19
10.	Initial estimates of general code parameters. ....	20
11.	Grout and soil distribution coefficients and bounding aqueous-phase and free-air diffusivity values. ....	21
12.	van Genuchten-Mualem model parameters for relative permeability and capillary pressure. ....	26
13.	Solubility and non-solubility limited contaminants of potential concern. ....	28
14.	Activity, half-life, and molecular weights of radiological COPCs. ....	31
15.	Nitrate-containing chemicals in Subsurface Disposal Area waste and total estimated nitrate inventory. ....	32
16.	Estimated inventory of contaminants of potential concern in Subsurface Disposal Area waste. ....	32
17.	Estimated waste zone areas, waste zone volumes, and water mass for each COPC. ....	33
18.	Estimated contaminant of potential concern mass fractions. ....	34
19.	Contaminant of potential concern mass released from grout waste monolith during 10,000 years. ....	37
20.	Grout waste model moisture content. ....	41
21.	Mass remaining of Tc- 99 as increased resolution in the horizontal. ....	42
22.	Mass release subject to vertical and horizontal grid refinement. ....	43
23.	Percentage of mass released of GenRad with varying permeabilities. ....	45
24.	Mass release from infiltration values of 0.185 and 1.85 cm/yr. ....	46
25.	Mass release of contaminants of potential concern from monolith at 1,000 years according to $K_d$ and half-life. ....	49
26.	Mass release of contaminants of potential concern at 10,000 years according to $K_d$ and half-life. ....	49
27.	Comparison of fracture volume and permeability. ....	50
28.	Percentage of mass released (GenRad) as the presence of fractures increases in the monolith. ....	51

## ACRONYMS

ANSI/ANS	American National Standards Institute/American Nuclear Society
COPCs	contaminants of potential concern
EOS	equations of state
INEEL	Idaho National Engineering and Environmental Laboratory
PGA	peak ground acceleration
RWMC	Radioactive Waste Management Complex
SDA	Subsurface Disposal Area
TOUGH	Transport of Unsaturated Groundwater and Heat code
VOC	volatile organic compound



# **Final Results Report, In Situ Grouting Technology for Application in Buried Transuranic Waste Sites Volume 2, Evaluation of Proposed In Situ Grouting of Operable Unit 7-13/14 Waste against Limited Feasibility Study Criteria**

## **1. DURABILITY AND PERFORMANCE OF GROUTED WASTE MONOLITHS IN THE SUBSURFACE DISPOSAL AREA**

### **1.1 Objective**

This document, Volume 2 of the *Final Results Report, In Situ Grouting Technology for Application in Buried Transuranic Waste Sites* (Loomis et al. 2002) fulfills in situ grouting treatability study Test Objectives 1 and 4, as stated in the *Test Plan for the Operable Unit 7-13/14 Bench-Testing In Situ Grouting Treatability Study* (Grant et al. 2000) and the *Implementation Test and Field Test Plan for the Operable Unit 7-13/14 In Situ Grouting Treatability Study* (Loomis, Jessmore, and Weidner 2001), in both estimating the durability of the grouted waste monoliths and evaluating the chemical buffering properties of the grouted waste form in the Subsurface Disposal Area (SDA). Estimates of both durability and chemical buffering were made separately through theory and analytical solutions. In addition, numerical simulations (results in Appendix A) were made to integrate these and other factors to produce mass release curves for each contaminant of potential concern. Numerical simulations were also performed to estimate the effects of freezing/thawing and seismic loading on a grouted waste monolith located at the SDA. The SDA is a 39-ha (96-acre) disposal area inside the Radioactive Waste Management Complex (RWMC), which is located in the southwest corner of the Idaho National Engineering and Environmental Laboratory (INEEL).

#### **1.1.1 Durability of Grouted Waste Monoliths**

Estimating the durability of cementitious waste forms, including grouted waste monoliths, is critically important in evaluating the effectiveness of grouting as a remedy in treating radioactive and other wastes. Significant research has been and continues to be undertaken to address this subject. Despite such efforts, current understanding of the fundamental mechanisms of governing contaminant release do not justify the extrapolation of current short-term tests to time spans as long as 10,000 years.<sup>a</sup> In fact, an accepted definition of durability, as it relates to this subject, has yet to be articulated. Despite this lack of quantitative clarity, various organizations are working to more rigorously define the concept. The International Atomic Energy Agency is one, and has published various technical reports on this subject. These include Technical Report Series No. 350 *Improved Cement Solidification of Low and Intermediate Level Radioactive Wastes* (1993) and No. 187 *Characteristics of Solidified High-Level Waste Products* (1979). Conner's (1990) text, *Chemical Fixation and Solidification of Hazardous Waste* also includes information relevant to durability. The Nuclear Regulatory Commission Topical Position Paper of 1991 recommends several tests for durability. However, these tests are short-term (up to 90 days) and are limited in value and applicability. Several European researchers are addressing durability. Led by Dr. Hans van der Sloot (Netherlands Energy Research Foundation) and working with Dr. David Kosson (Vanderbilt), they use the principles of the Kosson protocol developed for the U.S. Environmental

---

a. Roger Spence, Oak Ridge National Laboratory researcher, personal communication with Eric Miller, INEEL, April 7, 2003).

Protection Agency. Dr. Julia Stegemann (Imperial College London Concrete Durability Group) is another European researcher addressing the concept of durability. In the U.S., Dr. Roger Spence, Oak Ridge National Laboratory, has authored several papers relating to durability and is considered a leading expert.

Other researchers have attempted to extrapolate the results of short-term experimentation to long-term durability by using the concepts of natural cementitious analogs. A fair amount of information is available on the longevity of archaeological cements and concretes and the evolution of the mineralogy in such materials. Natural analogs are particularly useful for testing chemical thermodynamic models or radionuclide solubility and speciation. In addition, analog studies can also indicate possible perturbations caused by microbes, organics and colloids (McKinley and Alexander). However, significant technical hurdles remain that preclude the use of analog data to both define and quantify the durability of modern cementitious materials.

Despite the work of experts, an accepted method to estimate concrete durability does not presently exist. The current state-of-the-art is to satisfy existing regulatory criteria by a simple measure of leach resistance, such as Toxicity Characteristic Leaching Procedure, American National Standards Institute/American Nuclear Society (ANSI/ANS) 16.1). This, along with the Nuclear Regulatory Commission Topical Position Paper of 1991, represents the most extensive set of durability tests quoted by a regulatory agency.

Test Objective 1 indicates that the performance lifetime of the grouted waste monoliths will be calculated from (ANSI/ANS 16.1 leach data (1986) to estimate the long-term physical and chemical durability of the grouted waste (Loomis, Jessmore, and Weidner 2001). Three chemical indicators were identified in Test Objective 1 to provide quantitative measures of the effective diffusion coefficient, from which a “leachability index” was then calculated. The ANSI/ANS 16.1 standard provides a uniform procedure to measure and index the release of radionuclides from waste forms, as a result of leaching in demineralized water. Demineralized water is chosen as the leachant because it is more aggressive than the native ground water. Typically, groundwater is high in calcium, magnesium, carbonates, aluminates, and silicates that coat the soil-grout surface and slow leaching. Experience has shown that conservative estimates of the contaminant releases based on effective diffusion coefficients from this method are 25-100 times higher than actually observed in the field. The ratio of the demineralized water volume to the waste forms external geometric surface area is maintained within fixed bounds. Samples of the water are collected at prescribed periods and tested for chemical constituents, and contaminant levels in the leachate water are determined for those periods. The data are then used to calculate the diffusion constant of the contaminant in the waste form. It is expressed as the leaching index, which is a negative natural logarithm of the ratio of the diffusion constant. The three chemical indicators were calcium, aluminum, and silicon. Average leachability index results for these three indicators for each of the five neat grout tests are found in Table 1.

Table 1. Average leachability index results for each of the five neat grout tests.

Grout	Calcium Leachability Index	Aluminum Leachability Index	Silicon Leachability Index
US Grout	11.45	11.75	9.90
TECT-HG Grout	10.85	12.44	11.52
Enviroblend Grout	10.07	16.00	15.67
GMENT-12 Grout	10.81	12.00	10.07
Salt Stone Grout	11.57	12.90	10.11

The leachability indexes in Table 1 reflect the leachability in neat grout. However, in the SDA grouted wastes, materials (e.g., organics, nitrate salts, and soils) will be present that may either enhance or retard leachability relative to neat grout. Leachability experiments were performed for three such potential interferences using strontium as the indicator species. Leachability indexes for strontium in neat grout, along with leachability indexes for strontium in the presence of potential interferences, can be compared to determine if significant interferences can be expected. In addition, this information can be used as a scaling factor to estimate the leachability of other species (e.g., calcium, aluminum, and silicon) in grouted waste. Table 2 contains leachability index information for strontium for neat grout and for mixtures of neat grout with organics, nitrate salts, and soil for each of the five test grouts.

Table 2. Leachability index for strontium for neat grout and neat grout with organics, nitrate salts, and soil for each of the five test grouts.

Grout	Neat Grout	9% Organics	12% Nitrate Salts	50% Soils
US Grout	12.02	11.37	11.77	12.63
TECT-HG Grout	10.43	9.70	10.73	10.87
Enviroblend Grout	13.10	13.10	13.90	13.83
GMENT-12 Grout	10.04	10.57	10.77	10.80
Salt Stone Grout	11.06	10.77	10.57	10.97

As can be noted from Table 2, the presence of organics in the waste material generally appears to reduce the leachability index (i.e., increased leachability), while the presence of nitrate salts and soils tends to retard leachability. However, given the small volumetric fractions of organics and nitrate salts thought to be present in the waste (i.e., 5.9% and 4.3%, respectively), it is likely that the effective leachability indexes for actual grouted waste are similar to, if not marginally higher than, those measured for the neat grout for each grout type.

Although no recognized method of estimating grout durability directly from leachability indexes currently exists, leachability indexes do provide a means for estimating the amount of time required to remove given fractions of the original material. Percent mass retention estimates can be made based on an analogous heat transfer analytical solution (Carslaw and Jaeger 1959) for heat conduction in a cylindrical slab. The basic form of the differential equation used in this estimate is:

$$\frac{\partial v}{\partial t} = k \frac{\partial^2 v}{\partial x^2} \tag{1}$$

where

v = temperature

t = time

x = slab thickness

k = thermal conductivity.

The solution to Equation (1) for a slab of thickness  $-l < x < l$  with constant initial temperature,  $V_0$ , in terms of average temperature,  $v_{av}$ , in the slab at any time, (t), is given by:

$$V_{av} = \frac{8V_0}{\pi^2} \sum_{n=0}^{\infty} \frac{1}{(2n+1)^2} \ell^{-\left[\frac{k(2n+1)^2 \pi^2 t}{(4l)^2}\right]} \quad (2)$$

Dividing each side of Equation (2) by  $V_0$  gives  $V_{av}/V_0$  on the left side of this expression, which, when multiplied by 100, provides the percent of original temperature (i.e., mass) remaining in the slab at times of interest. Using this expression, along with reported leachability index values from Table 1 converted to effective diffusion coefficients, the mass of calcium, aluminum, and silicon remaining in each grout at 1,000, 10,000, and 100,000 years can be estimated. These estimates are found in Tables 3 through 5.

Table 3. Percent of original calcium remaining in neat grout at select times.

Grout	1,000 Years	10,000 Years	100,000 Years
US Grout	88	63	5.5
TECT-HG Grout	77	28	Less than 1%
Enviroblend Grout	43	Less than 1%	Less than 1%
GMENT-12 Grout	75	25	Less than 1%
Salt Stone Grout	90	68	11

Table 4. Percent of original aluminum remaining in neat grout at select times.

Grout	1,000 Years	10,000 Years	100,000 Years
US Grout	92	74	21
TECT-HG Grout	96	88	62
Enviroblend Grout	99	99	99
GMENT-12 Grout	94	80	38
Salt Stone Grout	98	93	78

Table 5. Percent of original silicon remaining in neat grout at select times.

Grout	1,000 Years	10,000 Years	100,000 Years
US Grout	31	Less than 1%	Less than 1%
TECT-HG Grout	89	66	8.2
Enviroblend Grout	99	99	99
GMENT-12 Grout	43	Less than 1%	Less than 1%
Salt Stone Grout	45	Less than 1%	Less than 1%

These estimates are likely to be conservative for two reasons. First, these estimates assume that the diffusion of each chemical would occur in demineralized water. The SDA groundwater contains significant amounts of both calcium and silicon, which would likely coat the grout surface and slow the leaching. Second, the estimates are based on a physical geometry consisting of a circular disk with a radius of 10 in. and a thickness of 1 in. This geometry represents an extreme scenario where monoliths would experience significant cracking at the time of grouting.

### 1.1.2 Monolith Cracking

Although it is extremely unlikely that a grouted waste monolith in the SDA would crack immediately following its placement, the greatest long-term weakness of concrete (monoliths) for radioactive waste isolation is its tendency to crack (NUREG 1992). The degree to which the grouted monolith will crack and when such cracks appear during the life of the monolith will greatly affect the rate of contaminant mass release. However, precise crack predictions in concrete are very difficult, even under controlled laboratory conditions (Winkel 1992). In general, the overall scenario for concrete degradation begins with cracking related to drying shrinkage and temperature change. These initial mechanisms for cracking generally are followed by overall degradation of the concrete. Sulfate attack, reinforcement corrosion, leaching, and other means cause permeability to gradually increase and lead to the development of further cracks. These processes are estimated to take place over several hundred to several thousand years (NUREG 1992). Ultimately, the concrete will become “rubble,” at which time it will have lost much of its resistance to flow, but will retain some of the original chemical buffering properties. This general progression for concrete occurs in the absence of waste. Applying grouted monoliths to low-level radioactive waste because of its intrinsic ionizing radiation, may introduce further structural changes (e.g., embrittlement) that may have dramatic effects on mechanical properties of the waste (Huang, Mitchell, and Conner 1993).

## 1.2 Impacts of Freeze/Thaw and Seismic Activity on Grouted Monoliths in the Subsurface Disposal Area

Given the sensitivity of monolith performance to cracking, it is natural to question the impacts of both freezing/thawing of an uncovered monolith (Appendix B) and seismic loading (Appendix C) on monolith crack formation and propagation. According to the Uniform Building Code, the INEEL is in Seismic Zone 2B, meaning that moderate damage could occur as a result of an earthquake. Historic and recent seismic data catalogued by the National Oceanic and Atmospheric Administration and the National Earthquake Information Center indicate that earthquakes within the region occur primarily in the Intermountain Seismic Belt and the Centennial Tectonic Belt. The seismic characteristics of the INEEL’s Eastern Snake River Plain and the adjacent Basin and Range Province are different, and the plain has historically experienced few and small earthquakes (Woodward-Clyde Federal Services Geomatrix Consultants and Pacific Engineering Analysis 1996). Earthquake monitoring by the INEEL and other seismic networks shows that the Eastern Snake River Plain and adjacent parts of the nearby mountain ranges form a seismic zone of inactivity or relatively low seismic activity. An earthquake with a maximum horizontal acceleration of 0.15 g is calculated to have an annual probability occurrence of 1 in 5,000 at the INEEL site (Woodward-Clyde Federal Services Geomatrix Consultants and Pacific Engineering Analysis 1996). Furthermore, empirical data suggest that seismic motions do not significantly affect subsurface structures (e.g., grouted monoliths) unless the peak ground acceleration exceeds about 0.3 g (Miller and Constantino 1994). The INEEL Seismic Hazard Curve for the Idaho Nuclear Technology and Engineering Center, Test Reactor Area, Radioactive Waste Management Complex, and Power Burst Facility indicates that the peak ground acceleration (PGA) of 0.3 g is calculated to have an annual probability occurrence of approximately 1 in 100,000. Soil heterogeneities resulting from local soil discontinuities, as are present in SDA alluvium, also are found to have little effect on the seismic response of subsurface structures. In addition, Miller and Constantino (1994) found that seismic-induced soil pressures vary in a near linear manner over the wall depth on a shallow, buried structure. They determined that the maximum pressures occur near the top of the structure. The resultant force from the soil pressure acts at a distance of about 60% of the wall height above the base. The significance for low-level radioactive waste buried in grouted monoliths is that the majority of the seismic-induced force is directed away from the monolith’s bottom surface where primary contamination release takes place.

## 2. CHEMICAL BUFFERING PROPERTIES OF THE GROUTED WASTE FORM

Test Objective 4 indicates that the solubility of each of the contaminants of potential concern will be computed as a function of Eh and pH in an aqueous solution similar to groundwater at the SDA, namely saturated with calcite and in equilibrium with CO<sub>2</sub> in the air (Loomis, Jessmore, and Weidner 2001). Although changes in the chemical properties of concrete over time will affect both the solubility and sorption of contaminants, the effect of concrete chemical property changes on sorption will not be computed in this study.

Geochemical reactions—in solid, liquid, and gaseous phases—will occur between waste components in the SDA subsurface and the various geochemical constituents present in the nonwaste materials like concrete. Such reactions will largely tend to retard the release of contaminants relative to release rates when no geochemical reactions occur. Thus, these geochemical reactions can be controlled to some extent and can be used to further retard contaminant migration beyond the benefit provided by grouting itself. The potential benefit of such chemical buffering in grouted waste systems can be significant. Specific examples of such reactions include secondary mineralization of calcium carbonate to “self-heal” existing cracks, incorporation into the crystalline lattice structure of cement hydration products, retardation through chemisorption or adsorption at hydrous surfaces, and solubility reduction of dissolving waste species into grout pore liquids. The nature and rate of these reactions will be specified by a complex set of factors, including the species present in the waste and the grouted matrix, temperature, pressure, pH, and Eh. Of particular interest is the control of contaminant solubility, because it represents the final “line of defense” in aqueous-phase contaminant release. Solubility refers to the total amount of an element or compound that can remain in solution under a specified set of conditions in the presence of an excess amount of the element in a solid phase of definite composition and crystal structure (Hull and Pace 2000). To estimate solubility for a mineral phase, the following information is needed:

- The concentrations of other species that participate in the reaction
- The mineral phase that will control solubility
- The pH of the solution
- The oxidation/reduction potential (i.e., Eh) of the solution.

For mineral species, the mineral-phase controlling solubility will be known as a result of empirical data relating to the grout formulation. In addition, it can also be conservatively assumed that there are no competing species that would tend to maximize solubility of a given species. Thus, the degree of geochemical retardation of a given component with a geochemical system can be estimated by characterizing the degree of pH and Eh change of that system and comparing respective solubility limits.

### 2.1 pH/Eh and Contaminants of Potential Concern Solubility in the Subsurface Disposal Area Subsurface

#### 2.1.1 Pre-grout Ph/Eh in the Subsurface Disposal Area

Natural waters, like those in SDA soil water that are pH controlled by the equilibrium between CO<sub>2</sub> (g) in the atmosphere, calcite(s), and carbonate (aq), will have a pH between 7.2 and 8.2 depending on the partial pressure of CO<sub>2</sub> (g). On average, the pH of pore water is approximately 7.2 (Hull and Pace 2000). At this pH, the Eh at 25°C can be estimated from the following equation:

$$Eh = 0.0148 \times [\log O_2 (aq) - 4pH + 86.08] \text{ (volts)} \quad (3)$$

where:

Eh = Redox potential (volts)

O<sub>2</sub> (aq) = concentration of oxygen in solution (moles/liter)

pH = pH of the solution.

Water at 25°C can retain a concentration of  $2.6 \times 10^{-4}$  moles/L (Manahan 1994) of oxygen. Therefore, assuming that water in the SDA is in communication with enough oxygen in soil gas to provide  $2.6 \times 10^{-4}$  moles/L, the Eh of SDA pore water is calculated to be approximately 800 mV at a pH of 7.2. However, biodegradable material in buried waste may result in significant biological activity in the SDA subsurface. Such activity may consume available oxygen and lower the aqueous phase concentration of oxygen in SDA soil gas and its Eh. In the absence of soil gas data, a precise estimate of the actual Eh conditions is difficult, however. Table 6 contains solubility data for identified COPCs assumed to represent the conditions of SDA pore water at a pH of 7 and Eh of 800 mV.

Table 6. Estimated solubilities of Subsurface Disposal Area contaminants of potential concern at pH 7 and Eh of 800 mV.

Metals	Solubility <sup>a</sup> (mg/l) at 800 mV
Ac	1.50E-06
Am	1.61E-06
C	1.35E+02
Cl	unlimited
Cs	unlimited
I	unlimited
Nb	1.45E-12
Np	6.33E-02
Pa	1.76E+03
Pb	3.88E-04
Pu	8.08E-09
Ra	9.71E-03
Sr	1.17
Tc	1.59E+4
U	9.32E-01
Inorganics	
nitrates	unlimited
Volatile Organic Compounds	
Carbon tetrachloride	733
Methylene chloride	22,920
Tetrachloroethylene	229

a. Solubility taken from Hull and Pace (2000)

Although data does not presently exist to determine the precise Eh of the SDA, the sensitivity of solubility to reductions in Eh that would be facilitated by possible microbial activity can be discussed. If the actual Eh is assumed to be slightly reducing at -100 mV, the majority of the COPCs solubilities are unchanged from those estimated at an Eh of 800 mV. Exceptions are plutonium, which decreases in

solubility by less than 1 order of magnitude, uranium, which decreases by more than 2 orders of magnitude, neptunium and protactinium, which decrease by more than 3 orders of magnitude, and technetium, which decreases by more than 12 orders of magnitude, moving from 800 mV to -100 mV at a pH of 7.

### **2.1.2 Post-grout Eh/pH and Contaminants of Potential Concern Solubility in Subsurface Disposal Area Waste**

As reported in Volume 1, all grouts tested produced alkaline, moderately oxidizing solutions having a pH in the range of 10.9 (GMENT-12) to 11.4 (TECT-HG), and Ehs of approximately 225 mv (Salt Stone) to 390 mv (US Grout). The average values are approximately pH of 11 and Eh of 310 mv. As cementitious grouts age, the pH and Eh of the pore water will change as a function of various factors. With respect to pH, the dissolution of calcium silicate hydrogel and portlandite phases has an important role in buffering the pH of resulting pore fluids. Initially, the pH of cementitious grout is very high (e.g., 13.5) when controlled by the dissolution of free portlandite in the grout. Eventually, the portlandite is depleted and the pore fluid Ph decreases to approximately 10.5, where it is controlled by the dissolution of calcium silicate hydrogel. The timeframe over which the pH of the pore solution changes from 13.5 to that of groundwater is determined by the rate at which water migrates through the cement system (Krupka and Serne 2001). Atkinson et al. (1989) estimated that the pH of the near-field pore water would remain above 10.5 for several hundred thousand years for designs of radioactive waste disposal systems being considered in the United Kingdom. The major constituent that can influence the Eh of cement pore fluids is sulfur often used in the solidification of radioactive waste. The Eh conditions may also be lowered by the corrosion of iron containers (e.g., drums) grouted in the waste form (Ewart et al. 1988). Card (1977) indicates that 148,736 steel drums of TRU waste alone were buried in the subsurface. Such a mass of iron bearing drums can reasonably be expected to lower the Eh of grouted wastes in areas where steel waste drums were buried. In areas where burial consisted mainly of cartoned and boxed wastes, the Eh can be expected to be at or below the Eh of non-iron bearing neat grout (i.e., 310 mV) depending upon the amount of biodegradable material captured within the grouted waste. Rigorous quantification of the degree to which the presence of either iron-bearing materials or biodegradable materials will reduce the Eh below the average of 310 mV is beyond the scope of this study. However, a bounding estimate of the degree of Eh reduction may be made by assuming the co-existence of carbonate from natural waters and iron from steel drums would lead to a siderite ( $\text{FeCO}_3$ ) controlled system. In such a system the Eh, at a pH of 10.5 would be approximately -400 mV (Langmuir 1996). Therefore, a reasonable range for Eh of grouted SDA wastes may be from moderately oxidizing (i.e., 310 mV) to moderately reducing (i.e., -400 mV). The solubilities of grouted contaminants of potential concern (COPCs) will be estimated assuming a long-term pH of 10.5, Ehs of 310 mV and -400 mV, and assuming that the same mineral phases that control individual solubilities in ungrouted SDA materials also control solubility in the grouted waste form. These estimates, along with their respective solubility change factors with respect to pre-grout conditions (see Table 6), are found in Table 7.

## **2.2 Evaluation of the Chemical Buffering Properties of the Grouted Waste Form**

Comparing the solubility limits of specific contaminants under pre-grout SDA and the post-grout conditions, the degree to which proposed grouts may affect the solubilities of COPCs can be assessed.

Comparing pre-grout solubilities to post grout solubilities at pH 10.5 and Eh 310 mV, it is seen that 10 of the 19 species show little to no change in solubility. Four of the remaining 10 species, namely actinium, americium, niobium, and lead show increased solubilities following grouting. The remaining five (i.e., neptunium, protactinium, plutonium, strontium, and uranium) show decreased solubilities.

Table 7. Estimated solubilities of grouted COPCs at pH 10.5 and Eh of 310 mV and –400 MV, and associated solubility change factors with respect to pre-grout conditions (Hull and Pace 2000).

Metals	Solubility (mg/l) of grouted waste at pH=10.5 and Eh=310 mV	Solubility Change factor from Pre-grout solubility (pH=7 and Eh = 800 mV)	Solubility (mg/l) of grouted waste at pH=10.5 and Eh=-400 mV	Solubility Change factor <sup>a</sup> from Pre-grout solubility (pH=7 and Eh = 800 mV)
Ac	1.78E-04	-120	1.78E-04	-120
Am	1.90E-04	-120	1.9E-04	-120
C	1.12E+02	1.2	1.12E+02	1.2
Cl	unlimited	0	unlimited	0
Cs	unlimited	0	unlimited	0
I	unlimited	0	unlimited	0
Nb	1.48E-08	-10,200	1.48E-08	-10,200
Np	3.55E-5	1800	9.33E-13	7E+10
Pa	1.97E+02	8.93	3.74E-04	5E+06
Pb	5.83E-02	-150	5.83E-02	-150
Pu	3.21E-12	2520	3.19E-12	2520
Ra	1.10E-02	-1.2	1.10E-02	-1.2
Sr	2.79E-03	420	2.79E-03	420
Tc	1.61E+04	-1.01	1.60E-18	1E+20
U	3.32E-04	2800	9.28E-05	10,000
Inorganics				
Nitrates	unlimited	0	unlimited	0
Volatile Organic Compounds				
Carbon tetrachloride	733	0	733	0
Methylene chloride	22,920	0	22,920	0
Tetrachloroethylene	229	0	229	0

a. A negative Solubility Change factor denotes increased solubility relative to pregrout conditions.

The same comparison with respect to post-grout solubilities at pH 10.5 and Eh –400 mV yields similar results. In this case, 9 of the 19 show little to no change in solubility with the same four (i.e., actinium, americium, niobium, and lead) showing the same level of increased solubility. The remaining six species consist of the five species that previously showed decreased solubility (i.e., neptunium, protactinium, plutonium, strontium, and uranium) plus technetium. However, in the case of these six species, the magnitude of the solubility decrease is more dramatic. Thus, the overall effect on solubility of grouting SDA waste is not straightforward. What may be concluded is that the solubility of the majority of COPCs in waste may not be significantly affected by grouting. Grouting may, in fact, increase the solubility of some COPCs, namely, actinium, americium, niobium, and lead. Approximately 1/3 of the COPCs (i.e., neptunium, protactinium, plutonium, strontium, uranium, and technetium) show that grouting may be very effective in decreasing their solubility. Of these six species, all but strontium show a strong sensitivity of solubility to the Eh conditions. As a result, if future efforts further narrow the list of COPCs to include any of these five constituents, engineering grout to ensure a moderate to highly reducing environment may be very successful in further minimizing their solubility in the final waste form.

### 3. SOURCE RELEASE MODELING

#### 3.1 Modeling Objectives

Test Objectives 1 and 4, as stated in the *Test Plan for the Operable Unit 7-13/14 Bench-Testing In Situ Grouting Treatability Study* (Grant et al. 2000) and the *Implementation Test and Field Test Plan for the Operable Unit 7-13/14 In Situ Grouting Treatability Study* (Loomis, Jessmore, and Weidner 2001) identify the evaluation of grouted monolith durability and chemical buffering as separate test objectives. Although some of the factors (e.g., seismic effects) that effect monolith durability and chemical buffering are uniquely separate, many of these mechanisms are ultimately correlated with each other. Therefore, any rigorous evaluation of their combined effects will need to address such interrelations. As such, numerical modeling was selected as a means to supplement previously conducted empirical and theoretical evaluations of grouted monolith durability and chemical buffering and to more rigorously evaluate their combined effects.

The objective is to integrate the effects of grout durability and chemical buffering in a systematic way to create a more holistic evaluation. To achieve this overall objective, a series of implementing objectives were selected as follows:

- Estimate individual COPC mass release.
- Identify COPC critical release mechanisms.
- Estimate monolith saturation over time to infer monolith durability.
- Estimate COPC mass release sensitivity and uncertainty.
- Estimate maximum COPC soil concentrations beneath grouted waste for possible use in future groundwater contaminant screening activities.

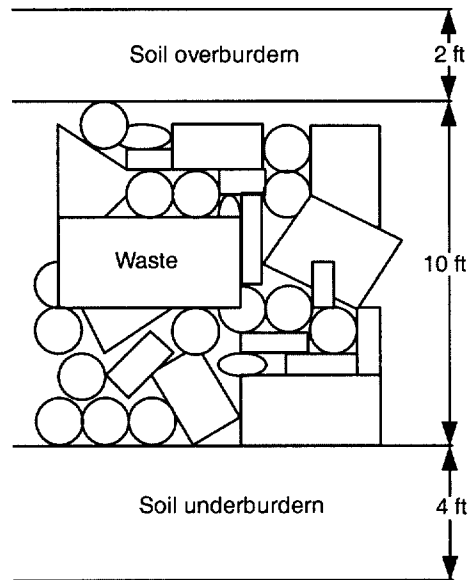
The COPCs for this modeling effort (see Table 8) were selected to be consistent with the contaminants of concern identified in the *Ancillary Basis for Risk Analysis of the Subsurface Disposal Area* (Holdren et al. 2002).

#### 3.2 Conceptual Model Development

The SDA is a 39-ha (96-acre) disposal area inside the RWMC. The near-surface geology of the SDA consists of surficial sediment deposits overlaying thick basalt deposits. Irregularities in the soil thickness, ranging from 0.6 to 7 m (2 to 23 ft) reflect the surface undulations of the underlying basalts (Anderson, Liszewski, and Ackerman 1996). The surface soils consist mainly of silty clays and sands (Arrenholtz and Knight 1991). From 1952 to 1970, solid, transuranic, and low-level wastes were buried in shallow waste disposal pits, trenches, and soil vault rows (Arrenholtz and Knight 1991). To construct the pits, surficial soil was excavated to competent basalt, and then backfilled with soil to provide a level floor (Guay 1989). (See Figure 1.) Guay reports the average thickness of soil left in place (i.e., underburden), the estimated waste thickness, and the average thickness of overburden soil for Pits 1,2,3,4,5,6,9, and 10. The average thickness of soil underburden, waste, and soil overburden, weighted by pit surface area, are 3.8, 9.6, and 6.0 ft. respectively. Overburden thicknesses calculated from Guay (1989) correlate well with neutron-moisture log analysis for Pit 9, which concluded that the Pit 9 overburden thickness generally is 1.2- to 1.8-m (4- to 6-ft) thick (EDF-ER-207). However, recent analysis of overburden thickness across the entire SDA based on subsidence data indicates that the overburden thickness varies widely, with an average of less than 0.6 m (2 ft) (Holdren et al. 2002). Although model predictions are likely insensitive

Table 8. Contaminants of potential concern.

Radionuclides	Inorganics	Volatile Organic Compounds
Ac-227	Nitrates	Carbon tetrachloride
Am-241		Methylene chloride
C-14		Tetrachloroethylene
Cl-36		
Cs-137		
I-129		
Nb-94		
Np-237		
Pa-231		
Pb-210		
Pu-239		
Pu-240		
Ra-226		
Sr-90		
Tc-99		
U-233		
U-234		
U-235		
U-236		
U-238		



03-GA50435-01

Figure 1. Characterization of waste buried at the Subsurface Disposal Area.

to the thickness of overburden given the imposed infiltration rate, the smaller value of 0.6 m (2 ft) was assumed to be marginally more conservative. Guay (1989) also reports an average pit length of approximately 201 m (660 ft), and average pit width of approximately 33 m (110 ft).

### 3.2.1 Physical Characteristics of Materials

**3.2.1.1 Physical Characteristics of Surface Soils.** Generally, soil in the southern INEEL consists of fine-grained eolian soil deposits with some fluvial gravel and gravelly sands (EG&G 1988). SDA soils have clay content of approximately 36% and silt content of approximately 56% (Chatwin et al. 1992). The intrinsic permeability of surficial soils at the SDA has been estimated from the geometric mean of measured hydraulic conductivity values to be approximately  $5.7E-13 \text{ m}^2$  (Borghese 1988).

**3.2.1.2 Physical Characteristics of Waste.** Waste buried in the SDA consisted of paper, cloth, wood, metal debris, concrete, asphalt, and various sludge. Waste burial began in 1952 and continued through 1970 (Miller and Varvel 2001). Waste originally was containerized in metal drums and plywood boxes that have been exposed to the environment for as many as 50 years. Loomis et al. (2002) estimated that volumetric fraction of drums, boxes, and cardboard in waste to be 46%, 33%, and 21%, respectively. Applying these values and other assumptions relating to the porosity of the various waste materials, Loomis (2002) estimated the total void volume of waste to be 60%.

### 3.2.2 Pertinent Site Hydrology

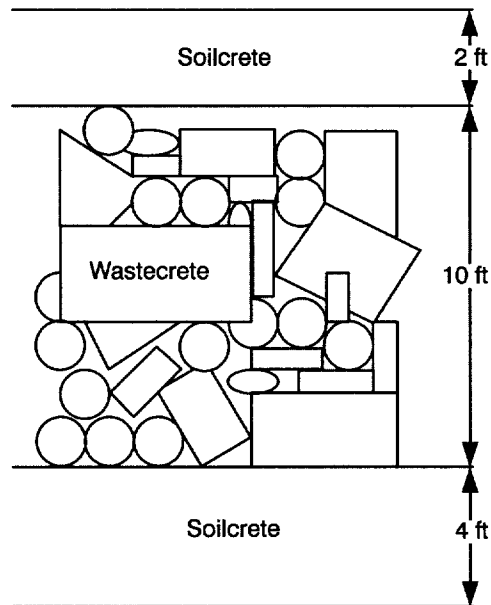
The region encompassing the RWMC is arid to semiarid (Clawson, Start, and Ricks 1989). Annual average precipitation at the INEEL is 22.1 cm (8.7 in.) with rates being the highest in May and June and lowest in July (Becker et al. 1998). The relatively dry climate and infrequent cloud cover result in large diurnal shifts in surface temperature. The average summer daytime maximum temperature is 28°C (83°F), while the average winter daytime maximum temperature is -0.6°C (31°F). Clawson, Start, and Ricks (1989) estimate the potential evaporation from saturated ground surface at the INEEL to be approximately 109 cm (43 in.). Actual evaporation rates are much lower than potential rates because the ground surface is rarely saturated (Becker et al. 1998). Periods when the greatest quantity of precipitation water is available for infiltration (late winter to spring) coincide with periods of relatively low evapotranspiration rates (EG&G 1981). Soil moisture infiltration rates at the RWMC vary widely depending upon location, material type, and timing of infiltration at the surface (Becker et al. 1998). Bishop (Holdren et al. 2002) reported wide variations in net infiltration from January 1994 through August 1996 based on the neutron access tube monitoring network. Over the monitored period, measurable net infiltration at the 22 neutron access tubes ranged from a high of 49 cm/year (19.4 in./year) to less than 0.3 cm/year (0.1 in./year). The wide range in net infiltration was attributed to a combination of variations in snow depth across the SDA, year-to-year variations in accumulated snowfall, spring drainage patterns of runoff and ponding, and proximity of the measurement locations to areas of runoff or ponding. Soil moisture ranges significantly with the seasons. Spring brings wetter conditions at the shallowest depths to approximately 1.2 m (4 ft). Deeper than 1.2 m (4 ft), the range of soil moisture is typically less variable. The soil moisture content throughout the profile ranges from 0 to 45% (McElroy 1993).

### 3.2.3 Grouting Protocol

Grouting of soil and waste materials would begin by first, driving a drill stem into the overburden and through the waste to refusal in the underlying basalt. On reaching basalt, the high-pressure grout injection pumps are started and the rotating drill string is withdrawn in discrete steps. Grout is pumped into the underburden, waste, and overburden through the rotating drill string until the surface is reached (Loomis et al. 2002). The resulting operation will create three distinct layers of material. Above and beneath the waste will be layers of grouted soil (i.e., soilcrete) surrounding a layer of grouted waste (i.e.,

wastecrete). A fourth layer, which may or may not be present, is a small soil layer that may remain resulting from the physical design of the drill stem and possible delays in grout injection after drill stem extraction is initiated. Planning estimates indicate the grouting would be nearly continuous, which could result in competent monoliths the length and width of the pits themselves (i.e., hundreds of feet).

Figure 2 shows the idealized grouted waste monolith.



03-GA50435-04

Figure 2. Matrix profile following grouting.

### 3.2.4 Contaminant Transport Mechanisms

Water flow and contaminant fate and transport are considered only for a conceptualized grouted source release zone (i.e., pit). Outputs of this source release model are to be used as inputs into existing vadose zone and groundwater simulations. Before establishing a formal conceptual model and entering into code selection, several planning sessions were held to prioritize potential transport mechanisms and factors effecting flow and transport. The following were the significant factors thought to effect flow and contaminant mass transport in this system:

- Initial concentration of contaminant mass
- Moisture infiltration rate and retention in monolith
- Initial monolith fracture density
- Chemical partitioning and solubility
- Temporally variable monolith transport characteristics (e.g., hydration, self-annealing, freeze/thaw, chemical leaching, seismic)

This information, along with other factors, including the type of waste (e.g., volatile organic compounds [VOCs]), matrix characteristics, near-surface hydrology, and grouting protocol, formed the

basis for the conceptual site model. As a result, the general flow model considered both aqueous and gaseous phase advection and diffusion of water into and out of the soilcrete and wastecrete materials, both laterally and vertically. Soilcrete materials were considered as homogenous, isotropic, porous media, presumably free of fractures. Wastecrete materials were considered as homogeneous, isotropic, interactive dual porosity media with the unique parameters being attributed to both a matrix and fracture media. Contaminant fate and transport mechanisms considered were aqueous phase advection and vapor phase diffusion both into and out of the soilcrete and wastecrete materials. Free phase contaminant transport was not considered because any significant free phase transport from source release zone was assumed to have already occurred and the jet grouting would not facilitate further free phase migration.

### **3.3 Assumptions**

This section contains a list of assumptions that offer further understanding of factors affecting hydrodynamic flow and contaminant transport. The assumptions are separated into flow modeling and transport modeling categories.

#### **3.3.1 Flow Modeling Assumptions**

- A flow gradient was not established between the vertical boundaries of model, and thus, it is assumed that horizontal flow will be negligible; whereas, the dominant flow within the model is in the ‘z’ direction because of infiltration and gravimetric forces.
- Although disproportionate liquid saturations exist within the matrix of the model, namely the 100 % saturation of the grout and grout/waste zone, the intrinsic permeability of these materials ( $10^{-17} \text{ m}^2$ ) will inhibit any flow, and gravimetric forces will overcome any lateral flow that may develop from these zones.
- Precipitation, modeled as infiltration, was constrained to the top of the active model domain.
- The baseline infiltration rate of 0.037 cm/yr represents the expected amount of moisture moving through the barrier or “capped” cover over the monolith (EDF-279). Fractures are limited to layers of grout and grout/waste and continue vertically through both layers as a uniform continuum. The fractures will be the source for global flow through the model.

#### **3.3.2 Transport Modeling Assumptions**

- Transport model analysis of total mass release requires simulations to be conducted as a single component rather than multi-component analysis. This approach eliminates multi-component interactions that prevent maximum dissolution of components into the aqueous phase, thereby reducing the potential for total mass release of a single component.
- Modeling total mass release from the monolith requires the maximum aqueous phase concentrations to be used as initial loading values and assumes all contaminant is in contact with the liquid saturation of the matrix. The contaminant also is considered to be homogeneously mixed throughout the monolith with no gaps or voids.

- Materials property assignments for grout/waste are assumed to be similar to grout/soil characteristics because data about mixed waste with grout is lacking. This approach gives conservative mass release estimates from the monolith because the intrinsic permeability of grout/soil is  $10^{-17} \text{ m}^2$ .
- Because hydrodynamic dispersion is caused by heterogeneities in the medium that create variations in flow velocities and flow paths, and the grout/waste medium is considered to be a homogeneous mixture of waste without voids, dispersion is not considered.
- Because diffusion occurs in tight and low permeable soils and clays with very low flow velocities, it is expected that diffusion will affect lateral transport of contaminant. However, because vertical flow will dominate hydrodynamic characteristics through advection, very small quantities of contaminants released laterally are not expected to affect overall mass release estimates from the monolith.
- Advection, sorption and radioactive decay are the parameters contributing to aqueous phase contaminant moving through the monolith and soil.
- A linear equilibrium reversible partition coefficient describes the geochemical processes of aqueous phase contaminant and media sediment.

### 3.4 Simulation Code

The Transport of Unsaturated Groundwater and Heat (TOUGH2) code (Pruess et al. 1999) was developed at the Lawrence Berkeley National Laboratory and is ideally suited for geothermal reservoir engineering, environmental assessment, remediation and nuclear waste isolation studies. The TOUGH2 code is a general-purpose numerical simulation program for multi-dimensional (1D, 2D and 3D) fluid and heat flow of multiphase, multi-component fluid mixtures in variably saturated media and aquifers. TOUGH2 incorporates a finite difference modeling approach for determining numerical solutions to mass and energy balances of fluid and heat flow. TOUGH2 code uses a number of equations of state (EOS) modules, which describe particular multiphase, multi-component flow and transport characteristics.

The EOS7R EOS module of TOUGH2 numerically describes radionuclide transport through porous and fractured media. The module is used when transport is defined by advection and molecular diffusion. The module incorporates the effects of first order decay and adsorption onto solid phase media when forming numerical solutions for chemical flow and transport. Hydrodynamic dispersive transport can be described when the EOS7R module is coupled with a dispersion module called T2DM; however, this arrangement is restricted to two-dimensional rectangular Cartesian domains (Oldenburg et al. 1995). Because the grout waste monolith project has been defined within a three-dimensional Cartesian domain, hydrodynamic dispersion will not be included in solutions of flow and transport of chemicals.

The VOCs can be modeled with the same equation of state module. However, because the EOS7R module incorporates a half-life input parameter and VOCs lack half-lives, the input parameter for half-life is set to a very large value ( $1.0\text{E}+50$ ), which eliminates any decay activity incorporated into mass balance equations.

The TOUGH2 user's manual describes fracture flow using the dual-porosity concept. Matrix elements of lower permeability are embedded in a system of interconnected fractures. Global flow occurs exclusively through the fracture system and is described as an effective porous medium. Fluid flow in the matrix and between the matrix and fracture is secondary to flow in the fractures and is described by means of interporosity flow driven by pressure gradients between the matrix and fracture. Multiple phase

component flow that may exist within the matrix element and the matrix/fracture interface is determined by temperature, pressure and mass fraction gradients.

To accurately describe fluid flows based upon gradients, TOUGH2 incorporates the method of multiple interacting continua (Pruess et al. 1999). Resolution of these gradients is determined by a series of one-dimensional nested grid elements specified by the user. Figure 3 illustrates four adjacent elements with a nested grid configuration.

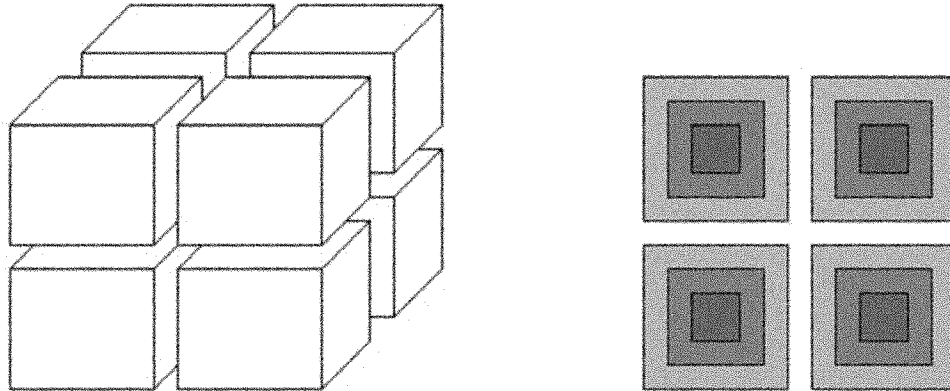


Figure 3. Matrix blocks in 3-D, and a 2-D representation of the nested grids within a matrix block.

TOUGH2 provides various formulations for defining tortuosity, including a relative permeability model, the Millington-Quirk model, and a constant diffusivity formulation. The current modeling applied the Millington-Quirk formulation.

Fluid flow from within the matrix toward a nearby fracture is modeled as migration through a series of gradients between each nested grid element, as seen in the shaded regions of the 2D drawing of Figure 3. Fractures are pathways between the blocks of nested grid elements. The distance from the fracture interface to each nested grid controls internal conditions within the nested grids of the matrix element.

Flow within the monolith is assumed to be dominant in the fractures and relatively minor in the matrix because of low permeability ( $10^{-17} \text{ m}^2$ ) values for the high-pressure injection grout.

### 3.5 Discretization

TOUGH2 handles flow geometry data by defining a list of volume elements or “grid blocks” and a list of flow connections between them. Each EOS module assigned with primary and or secondary thermodynamic variables identifies the phase condition of each element or grid block in reference to the volume of the element. The Cartesian coordinate positioning of the grid block becomes irrelevant and allows TOUGH2 modules to handle regular or irregular flow geometries in one, two and three dimensions.

The initial vertical grid block dimensions were derived from the estimated thicknesses of underburden, waste, and overburden established previously (Figure 1). The initial lateral dimensions of  $38.1 \text{ m}^2$  ( $125 \text{ ft}^2$ ) was chosen to be consistent with grid block sizes in Holdren (2002). Together, these dimensions provide the basis for the initial grid block geometry (Figure 4).

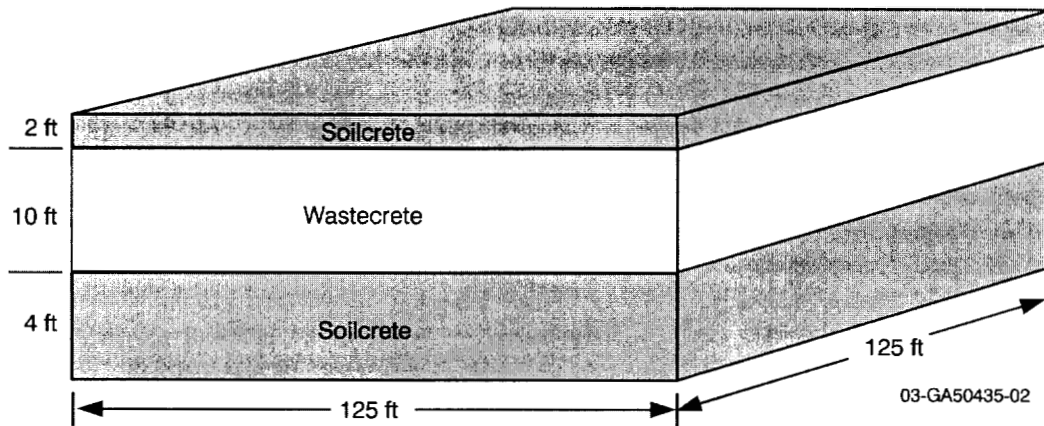


Figure 4. Initial grid block geometry.

To ensure better computational efficiency for fluid flow and contaminant transport, the ideal size or volume of the burial zone was arbitrarily reduced to  $72.58 \text{ m}^3$  ( $94.93 \text{ yd}^3$ ). This volume included a fourth soil underburden layer, which is theorized by some to exist at the basalt interface because of grouting protocol and equipment. In addition, this fourth layer was convenient to enable the model to predict near-surface soil contaminant concentrations for potential use in future soil-screening activities.

A simple, layered column was implemented as the grout waste monolith model design. The horizontal dimension of the column is  $8.52 \text{ m}^2$  ( $91.7 \text{ ft}^2$ ). Four divisions vertically divided the column and represented a soil cover (0.2 m [0.6 ft]), grout/waste zone (1.0 m [3.2 ft]), a grout/soil buffer zone (0.4 m [1/3 ft]) and bottom soil (0.4 m [1.3 ft]) layer (see Figure 5).

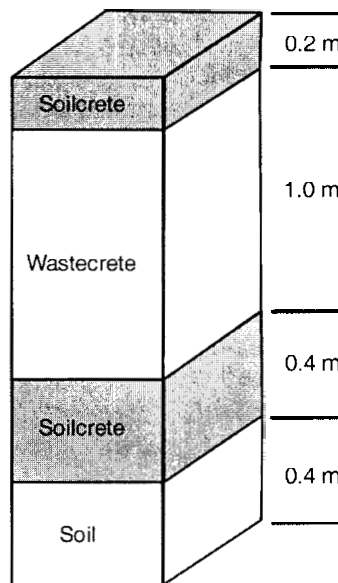


Figure 5. Grout waste monolith model design reduced scale.

The vertical dimensions maintained a relative scale to those estimated for the actual underburden waste and overburden layers. Creating a buffer zone of uncontaminated soil and grout to act as an insulative barrier inhibiting the escape of waste is anticipated during the grouting procedure and included in the model. Additional elements were positioned adjacent to each layer of the column as shown in Figure 6.

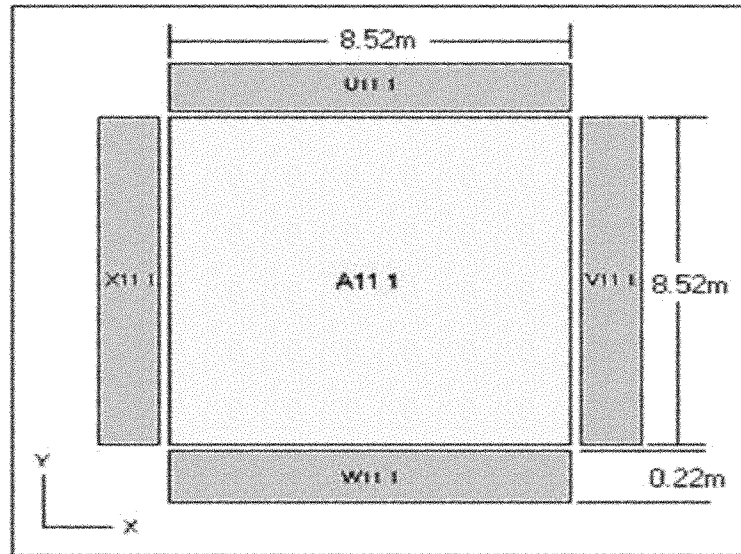


Figure 6. X-Y plane view of column A11 1 and adjacent elements (U-V-W-X11 1) of layer 1.

The material properties and dimensions of the adjacent elements matched the width and depth of each column layer, and were 0.22 m (0.7 ft) wide. The exceptions were elements adjacent to the grout/waste layer. These elements were assigned material properties of grout/soil and represented the same uncontaminated buffer zone previously defined. The final mesh modeled a central block of grout and contaminated waste, surrounded on sides and bottom with a zone of grout/soil mixture void of waste. The coarse grid discretization was necessary because of time constraints on the modeling activities. A more complex grid refinement originally was tried; however, attempts to achieve a reasonable water balance were unsuccessful. Identifying the cause of this problem was made difficult because of how complex the original grid discretization was. To identify the root cause of this problem, a more coarse grid discretization was constructed. Unfortunately, because of the volume of modeling work and the impending time constraints, further refinement of the grid discretization was sacrificed. A soil covering is above the central waste block and a layer of soil is at the base of the column. The bottom layer of soil was included in the design to anticipate obtaining ground soil concentrations of escaping waste.

### 3.6 Parameterization

To solve the governing equations in TOUGH2, the code requires establishing various parameters that describe the thermophysical properties of the system. Table 9 lists estimates of matrix parameters and their sources.

Table 9. Initial estimates of matrix parameters.

Parameter	Low	Average	High	Source
Wastecrete				
Monolith rock grain density (kg/m <sup>3</sup> )	2,216 kg/m <sup>3</sup>	2,310 kg/m <sup>3</sup>	2,951 kg/m <sup>3</sup>	Calculated values from neat grout densities and porosities
Monolith porosity		0.28		Verbal communication with Dr. Al Seihn, University of Akron, June 21, 2002
Monolith permeability	7.48E-18 m <sup>2</sup>	3.96E-17 m <sup>2</sup>	1.54E-16 m <sup>2</sup>	Calculated values based on measured hydraulic conductivities and the specific weight and dynamic viscosity of water
Van Genuchten-Mualem empirical shape factor ( $\alpha$ ) for grout		7.5E-07 cm <sup>-1</sup>		Walton and Seitz (1991) <sup>a</sup> and derived from data in Mikhail et al. (1964)
Van Genuchten-Mualem empirical shape factor (n) for grout		1.57		Walton and Seitz (1991) <sup>a</sup> and derived from data in Mikhail et al. (1964)
Surficial Sediments				
Soil rock grain density		3,000 kg/m <sup>3</sup>		Calculated value from Track 2 soil dry bulk density of 1.5 g/cm <sup>3</sup> and porosity of 0.5
Soil porosity		0.5		Martian (1995)
Soil permeability		6.71E-13 m <sup>2</sup>		Average of surface soil values from Martian (1995)
Van Genuchten-Mualem empirical shape factor ( $\alpha$ ) for soil		1.066 m <sup>-1</sup>		Baca et al. (1992)
Van Genuchten-Mualem empirical shape factor (n) for soil		1.523		Baca et al. (1992)

Table 9. (Continued).

Parameter	Low	Average	High	Source
Waste				
Waste density (pre-grout)		1,446 kg/m <sup>3</sup>		Verbal communication with Guy Loomis, May 14, 2002
Waste porosity (pre-grout)		0.6		Final Results Report–In Situ Grouting Technology for Application in Buried Waste Sites, Vol 1 (Loomis et al. 2002)
Neat Grout				
Neat grout density	1,600 kg/m <sup>3</sup>	1,806 kg/m <sup>3</sup>	2,160 kg/m <sup>3</sup>	Final Results Report–In Situ Grouting Technology for Application in Buried Waste Sites, Vol 1 (Loomis et al. 2002)
Neat grout porosity		0.25		Verbal communication with Dr. Al Seihn, University of Akron, June 21, 2002
a. Walton, J. C. and R. R. Seitz, 1991, “Performance of Intact and Partially Degraded Concrete Barriers in Limiting Fluid Flow (Draft),” NUREG/CR-5614, EGG-2614, Idaho National Engineering Laboratory, EG&G Idaho, prepared for the U.S. Nuclear Regulatory Commission.				

A specific tortuosity parameter was not explicitly specified for this simulation. The TOUGH2 has the capacity to internally calculate a porosity and saturation-dependent tortuosity from the Millington and Quirk (1961) model.

Table 10 provides general, nonmatrix specific parameters required for the TOUGH2 simulation. .

Table 10. Initial estimates of general code parameters.

Parameter	Low	Average	High	Source
Nonmatrix Parameters				
Domain temperature	4.5°C	9.75°C	15°C	Low and high at 2 m from Pittman (1989); mean is the average of the low and high.
Domain pressure	—	0.847 bar	—	National Oceanic and Atmospheric Administration average atmospheric data for 2001
Surface infiltration rate	0.037 cm/y	0.114 cm/y	49 cm/y	The high and average value from Holdren et al. 2002 the low value taken from EDF-279

Estimates of the distribution coefficients for each COPC in both grout and soil, as well as estimates of the most conservative aqueous-phase and free-air diffusivities are provided in Table 11.

Table 11. Grout and soil distribution coefficients and bounding aqueous-phase and free-air diffusivity values.

Category	Contaminant of Potential Concern	Grout Distribution Coefficient <sup>a</sup> (m <sup>3</sup> /kg)	Soil Distribution Coefficient <sup>b</sup> (m <sup>3</sup> /kg)	Aqueous-Phase Diffusivity (m <sup>2</sup> /s)	Free Air Diffusivity (m <sup>2</sup> /s)
Radionuclides	Ac-227	1.00E+00	1.50E+00	2.056E-09 <sup>c</sup>	
	Am-241	1.00E+00	9.60E+00		
	C-14	1.00E-01	2.30E-03		
	Cl-36	1.00E-03	0.00E+00		
	Cs-137	2.00E-02	9.50E-01		
	I-129	5.00E-03	1.60E-04		
	Nb-94	1.00E+00	5.00E-01		
	Np-237	2.00E+00	8.00E-03		
	Pa-231	5.00E+00	1.80E+00		
	Pb-210	5.00E-01	1.60E+01		
	Pu-239	5.00E+00	7.80E+00		
	Pu-240	5.00E+00	7.80E+00		
	Ra-226	5.00E-02	6.40E+00		
	Sr-90	1.00E-03	2.40E-02		
	Tc-99	0.00E+00	0.00E+00		
	U-233	1.00E+00	1.47E-01		
	U-234	1.00E+00	1.47E-01		
	U-235	1.00E+00	1.47E-01		
	U-236	1.00E+00	1.47E-01		
U-238	1.00E+00	1.47E-01			
Inorganics	Nitrates	0.00E+00	0.00E+00 0.00E+00		
Volatile organic compounds	Carbon tetrachloride	0.00E+00	0.00E+00		8.451E-06 <sup>d</sup>
	Methylene chloride	0.00E+00	0.00E+00		
	Tetrachloroethylene	0.00E+00	0.00E+00		

a. Distribution coefficients for grout were taken from Krupka and Serne (2001).

b. Distribution coefficients for soil were taken from Dicke (1997).

c. CRC 75<sup>th</sup> Edition.

d. Hazardous Waste Management (LaGrega et al. 1994).

It was assumed, for conservatism and convenience, that the individual COPC possessing the largest diffusivity in each diffusivity category (i.e., aqueous phase and free air) would be representative of all COPCs in that category because of the typically small range over which diffusion values vary.

Krupka and Serne (2001) provide distribution coefficient values for each COPC in three separate environments based on which dominates the pore water chemistry. In addition, for each of the three environments, distribution coefficients are provided for both an oxidizing and reducing condition. Environment II is the period in which soluble salts of the alkali metals are dissolved and the pH of the pore water is controlled by the solubility of portlandite. This environment is estimated to last from 100 to 10,000 years, to 1,000 to 100,000 years. Based on the time scale of this modeling effort (approximately 10,000 years) distribution coefficients from Environment II were selected. Oxidizing conditions were assumed for conservatism because of their marginally lower distribution coefficients than those listed for reducing conditions.

### 3.7 Boundary Conditions

Setting boundary conditions that accommodate potential flow gradients, both vertically and horizontally, can be easily performed within the architecture of TOUGH2. Boundaries are assigned variables such as pressure, temperature and saturation, which are similar to variables of the grid elements in the model. With respect to numerical computations, (i.e., mass or energy balance equations) the contents of the variables remain constant or unchanged throughout the simulation. Hydraulic flows are permitted to access the boundaries, either entering or exiting the model. Aqueous concentrations of contaminants are permitted to flow across model boundaries but not the reverse direction.

Because the model is defined within a vadose zone environment, gas or liquid saturation is the most influential variable for flow dynamics throughout the model and across its boundaries. A value of 50 % gas saturation was defined for the soil matrix, as well as for the bottom and lateral boundaries. While this is a conservative value, this creates a potentially aggressive flow gradient compared to the monolith gas saturation of zero. The top of the model was assigned a value of 100 % gas saturation representing the surface in contact with the atmosphere. Figure 7 shows a cross section of the monolith model, with initial gas saturation conditions.

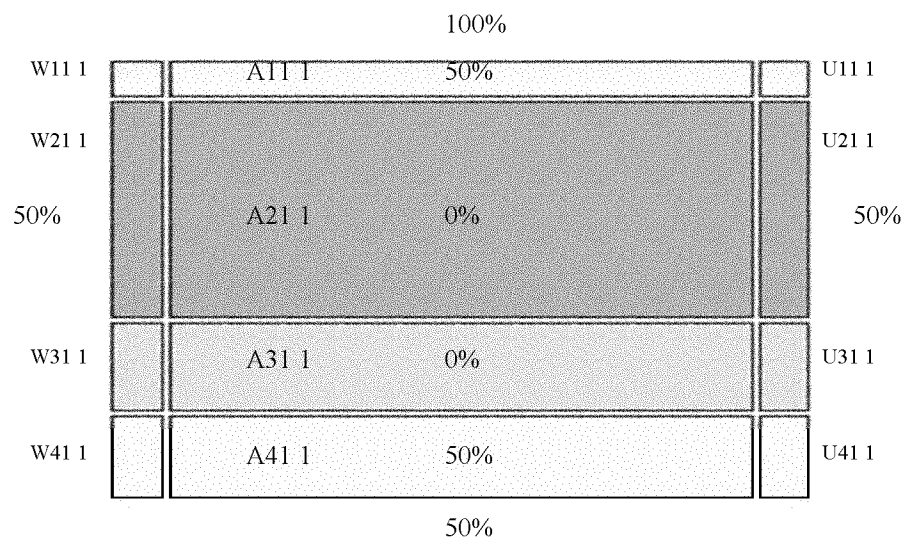


Figure 7. Gas saturation distribution of the grout waste monolith model.

Boundary variables for gas pressure and temperature are not expected to develop gradients as model depth increases, and do not influence flow dynamics. The goal was to mimic hydrodynamic flow in 3D, however, the model design casts doubt on whether 3D flow was ever modeled.

Fluid flow and contaminant transport through the model is anticipated to be primarily in the vertical direction with marginal horizontal flow. As noted previously, the anticipated infiltration rate is estimated to be 0.037 cm/yr (EDF-279), which assumes constant infiltration from an engineered cap.

Because of the low intrinsic permeability of the grout/waste element A21 1 (magnitude of  $10^{-17} \text{ m}^2$ ) and a relatively higher value for soil, (magnitude of  $10^{-13} \text{ m}^2$ ) a portion of infiltration, approximately 15%, will be diverted horizontally and therefore require lateral flow boundaries. Hydrodynamic flow established a symmetrical pattern immediately in the simulation, and reached steady state at approximately 500 years (see Figure 8).

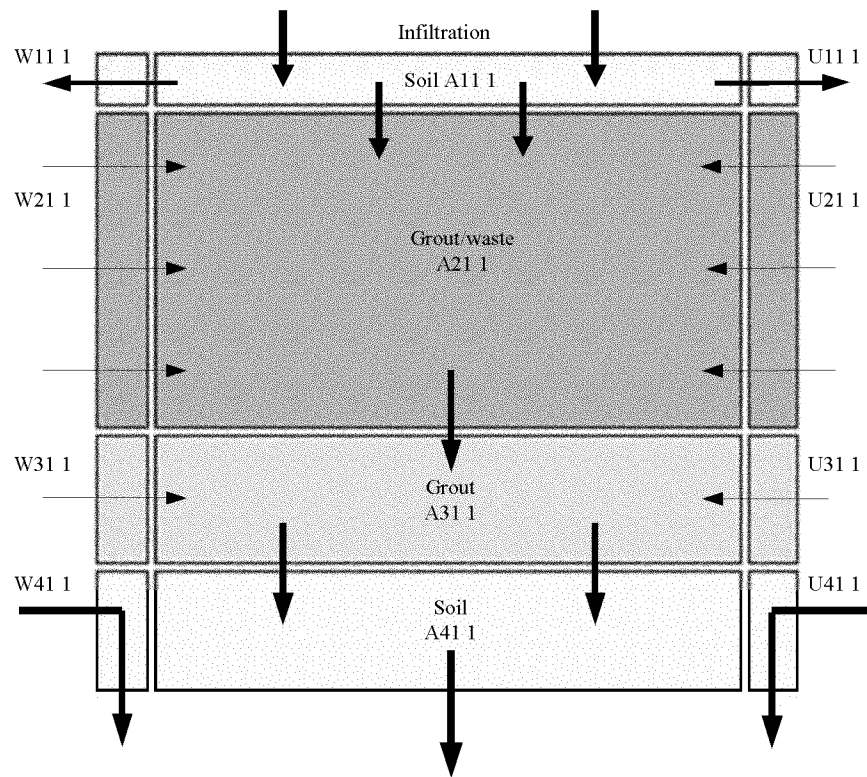


Figure 8. Cross section of the hydraulic flow patterns generated in the monolith.

The thickest arrows represent the greatest flows of infiltration in the vertical direction, with 15% redirected laterally to the side boundaries and 85% penetrating the grout/waste layer (A21 1) underneath. Vertical flow through the column continues to increase because of the contribution of side flows, albeit small, as shown in Figure 8. Considering that vertical flow is on the order of  $10^{-6} \text{ kg/sec}$  or approximately 86 ml/day, lateral flows from the side boundaries into the elements V21 1 & W31 1 (grout buffer layer) are 100 to 1000 times less ( $10^{-8}$  and  $10^{-9} \text{ kg/sec}$ ), suggesting these layers are impervious to liquid saturations of surrounding soil. Conversely, flow from the boundaries through side layer four X411 1 (soil) is greatest for lateral flows and comparable to the vertical flow with similar rate of  $10^{-6} \text{ kg/sec}$ .

As flow enters the bottom side layer X411 1, it combines with the vertical flow and continues downward with only a fractional amount, less than  $10^{-8} \text{ kg/sec}$ , moving into the middle base element A41 1. Vertical flow exiting base element A41 1 is less than 5% greater than flow entering the top of the

column, element A21 1, supporting the premise that vertical flow primarily is responsible for fluid flow and contaminant transport through the monolith. The 50% liquid saturation for the boundary establishes a gradient for lateral flow but contributes less than 5% to the overall vertical flow.

Figures 9 through 12 provide a detailed look at the flow pattern established between the volume elements of the monolith at 500 years. In each figure, the last column labeled FLO (LIQ.) provides flow values between elements under the column headings ELEM1 and ELEM2 at the right side of the figures. The flow pattern in Figure 9 is symmetrical around each of the layered elements A11 1 through to A41 1, as indicated by identical values for each of the four lateral surfaces (U-V-W-X11 1 to 411 1).

ELEM1	ELEM2	INDEX	FLOH (V)	FLOH/FLOF (J/KG)	FLOF (KG/S)	FLO(BRINE) (KG/S)	FLO(GAS) (KG/S)	FLO(LIQ.) (KG/S)
U11 1	A11 1	37	0.144645E-02	0.426271E+05	0.339325E-07	0.000000E+00	0.272833E-09	0.336597E-07
V11 1	A11 1	38	0.144645E-02	0.426271E+05	0.339325E-07	0.000000E+00	0.272833E-09	0.336597E-07
W11 1	A11 1	39	0.144645E-02	0.426271E+05	0.339325E-07	0.000000E+00	0.272833E-09	0.336597E-07
X11 1	A11 1	40	0.144645E-02	0.426271E+05	0.339325E-07	0.000000E+00	0.272833E-09	0.336597E-07
U21 1	A21 1	41	-.182331E-03	0.420758E+05	-.433340E-08	-.417798E-29	0.000000E+00	-.433340E-08
V21 1	A21 1	42	-.182331E-03	0.420758E+05	-.433340E-08	-.510385E-31	0.000000E+00	-.433340E-08
W21 1	A21 1	43	-.182331E-03	0.420758E+05	-.433340E-08	-.120864E-23	0.000000E+00	-.433340E-08
X21 1	A21 1	44	-.182331E-03	0.420758E+05	-.433340E-08	-.447220E-30	0.000000E+00	-.433340E-08
U31 1	A31 1	45	-.102099E-03	0.420757E+05	-.242656E-08	-.202974E-30	0.000000E+00	-.242656E-08
V31 1	A31 1	46	-.102099E-03	0.420757E+05	-.242656E-08	-.344124E-28	0.000000E+00	-.242656E-08
W31 1	A31 1	47	-.102099E-03	0.420757E+05	-.242656E-08	-.718533E-25	0.000000E+00	-.242656E-08
X31 1	A31 1	48	-.102099E-03	0.420757E+05	-.242656E-08	-.201285E-28	0.000000E+00	-.242656E-08
U41 1	A41 1	49	-.106198E-02	0.983835E+05	-.107942E-07	-.397755E-31	-.886082E-08	-.193342E-08
V41 1	A41 1	50	-.106198E-02	0.983835E+05	-.107942E-07	-.345617E-30	-.886082E-08	-.193342E-08
W41 1	A41 1	51	-.106198E-02	0.983835E+05	-.107942E-07	-.659079E-27	-.886082E-08	-.193342E-08
X41 1	A41 1	52	-.106198E-02	0.983835E+05	-.107942E-07	-.201094E-30	-.886082E-08	-.193342E-08

Figure 9. Horizontal flow values between the column and lateral elements.

A negative value indicates the direction of flow from ELEM 1 to ELEM 2, whereas a positive value indicates the reverse direction, from ELEM 2 to ELEM 1. Flow symmetry is maintained between elements interfaced with the column and side boundary as indicated in Figure 10. Figures 9 and 10 indicate that lateral flow in the top layer (U-V-W-X11 1) is directed away from the column, whereas lateral flow in the remaining layers move from the side boundary towards the column.

ELEM1	ELEM2	INDEX	FLOH (V)	FLOH/FLOF (J/KG)	FLOF (KG/S)	FLO(BRINE) (KG/S)	FLO(GAS) (KG/S)	FLO(LIQ.) (KG/S)
sid 0	U11 1	21	0.790519E-02	0.662165E+05	0.119384E-06	0.674965E-27	0.420160E-07	0.773679E-07
sid 0	V11 1	22	0.790519E-02	0.662165E+05	0.119384E-06	0.202503E-28	0.420160E-07	0.773679E-07
sid 0	W11 1	23	0.790519E-02	0.662165E+05	0.119384E-06	0.864849E-29	0.420160E-07	0.773679E-07
sid 0	X11 1	24	0.790519E-02	0.662165E+05	0.119384E-06	0.105361E-29	0.420160E-07	0.773679E-07
sid 0	U21 1	25	-.291044E-03	0.420756E+05	-.691718E-08	0.000000E+00	0.000000E+00	-.691718E-08
sid 0	V21 1	26	-.291044E-03	0.420756E+05	-.691718E-08	0.000000E+00	0.000000E+00	-.691718E-08
sid 0	W21 1	27	-.291044E-03	0.420756E+05	-.691718E-08	0.000000E+00	0.000000E+00	-.691718E-08
sid 0	X21 1	28	-.291044E-03	0.420756E+05	-.691718E-08	0.000000E+00	0.000000E+00	-.691718E-08
sid 0	U31 1	29	-.319490E-04	0.420756E+05	-.759324E-09	0.000000E+00	0.000000E+00	-.759324E-09
sid 0	V31 1	30	-.319490E-04	0.420756E+05	-.759324E-09	0.000000E+00	0.000000E+00	-.759324E-09
sid 0	W31 1	31	-.319490E-04	0.420756E+05	-.759324E-09	0.000000E+00	0.000000E+00	-.759324E-09
sid 0	X31 1	32	-.319490E-04	0.420756E+05	-.759324E-09	0.000000E+00	0.000000E+00	-.759324E-09
sid 0	U41 1	33	-.108349E-01	0.635514E+05	-.170491E-06	0.000000E+00	-.533780E-07	-.117113E-06
sid 0	V41 1	34	-.108349E-01	0.635514E+05	-.170491E-06	0.000000E+00	-.533780E-07	-.117113E-06
sid 0	W41 1	35	-.108349E-01	0.635514E+05	-.170491E-06	0.000000E+00	-.533780E-07	-.117113E-06
sid 0	X41 1	36	-.108349E-01	0.635514E+05	-.170491E-06	0.000000E+00	-.533780E-07	-.117113E-06

Figure 10. Horizontal flow values between lateral elements and side boundary.

Figures 9 and 10 show that lateral flow for each layer is varied, with the greatest rate in bottom layer 41 1 at  $0.1171 \times 10^{-6}$  kg/sec. The direction of flow is reversed in the top layer 11 1 compared with succeeding layers as indicated by a positive value in the FLO(LIQ) column. This is caused by infiltration redirected laterally by the low permeable ( $1 \times 10^{-17}$  m<sup>2</sup>) grout layer A21 1 underneath. Figure 11 shows

the vertical flow between layers one and two is  $0.7165 \times 10^{-6}$  kg/sec, and is less than the rate of infiltration ( $0.8511 \times 10^{-6}$  kg/sec) entering the top element A11 1. This suggests contaminant transport is dominated by advective and diffusive means in the vertical direction. Lateral diffusion of contaminant will be less significant to mass transport through the monolith as compared with vertical advective transport.

ELEM1	ELEM2	INDEX	FLOH (V)	FLOH/FLOF (J/KG)	FLOF (KG/S)	FLO(BRINE) (KG/S)	FLO(GAS) (KG/S)	FLO(LIQ.) (KG/S)
A11 1	A21 1	1	-.301452E-01	0.420756E+05	-.716454E-06	0.000000E+00	0.000000E+00	-.716454E-06
A21 1	A31 1	2	-.308742E-01	0.420758E+05	-.733776E-06	-.605599E-24	0.000000E+00	-.733776E-06
A31 1	A41 1	3	-.312828E-01	0.420757E+05	-.743488E-06	-.125890E-22	0.000000E+00	-.743488E-06
A41 1	bot 0	53	-.355304E-01	0.451662E+05	-.786660E-06	-.158848E-22	-.354433E-07	-.751217E-06

Figure 11. Vertical flow values of the column.

Flow symmetry was further substantiated by studying the flow in the vertical direction of the elements (U-V-W-X11-1 to 41 1) surrounding the column (see Figure 12).

ELEM1	ELEM2	INDEX	FLOH (V)	FLOH/FLOF (J/KG)	FLOF (KG/S)	FLO(BRINE) (KG/S)	FLO(GAS) (KG/S)	FLO(LIQ.) (KG/S)
U11 1	U21 1	9	-.237230E-04	0.420756E+05	-.563818E-09	-.491880E-29	0.000000E+00	-.563818E-09
V11 1	V21 1	10	-.237230E-04	0.420756E+05	-.563818E-09	-.147574E-30	0.000000E+00	-.563818E-09
W11 1	W21 1	11	-.237230E-04	0.420756E+05	-.563818E-09	-.630259E-31	0.000000E+00	-.563818E-09
X11 1	X21 1	12	-.237230E-04	0.420756E+05	-.563818E-09	-.767817E-32	0.000000E+00	-.563818E-09
U21 1	U31 1	13	-.132459E-03	0.420758E+05	-.314810E-08	-.303518E-29	0.000000E+00	-.314810E-08
V21 1	V31 1	14	-.132459E-03	0.420758E+05	-.314810E-08	-.370781E-31	0.000000E+00	-.314810E-08
W21 1	W31 1	15	-.132459E-03	0.420758E+05	-.314810E-08	-.878046E-24	0.000000E+00	-.314810E-08
X21 1	X31 1	16	-.132459E-03	0.420758E+05	-.314810E-08	-.324893E-30	0.000000E+00	-.314810E-08
U31 1	U41 1	17	-.623128E-04	0.420757E+05	-.148097E-08	-.123879E-30	0.000000E+00	-.148097E-08
V31 1	V41 1	18	-.623128E-04	0.420757E+05	-.148097E-08	-.210025E-28	0.000000E+00	-.148097E-08
W31 1	W41 1	19	-.623128E-04	0.420757E+05	-.148097E-08	-.438533E-25	0.000000E+00	-.148097E-08
X31 1	X41 1	20	-.623128E-04	0.420757E+05	-.148097E-08	-.122847E-28	0.000000E+00	-.148097E-08
U41 1	bot 0	54	-.983525E-02	0.610213E+05	-.161177E-06	-.240000E-29	-.445172E-07	-.116660E-06
V41 1	bot 0	55	-.983525E-02	0.610213E+05	-.161177E-06	-.208541E-28	-.445172E-07	-.116660E-06
W41 1	bot 0	56	-.983525E-02	0.610213E+05	-.161177E-06	-.397679E-25	-.445172E-07	-.116660E-06
X41 1	bot 0	57	-.983525E-02	0.610213E+05	-.161177E-06	-.121337E-28	-.445172E-07	-.116660E-06

Figure 12. Vertical flow values of lateral elements.

Saturation values through the monolith reached steady state conditions at 500 years and water remained very close to initial values assigned to the model. Layer two of grout waste and layer three of grout maintained 99% of the moisture during the simulation. The top layer of soil increased to approximately 71% saturation because of infiltration, and the bottom layer decreased to approximately 29% because of less moisture received from impermeable layers directly above. Figure 13 shows saturation values of the monolith at steady state conditions.

### 3.8 Initial Conditions

The TOUGH2 code provides multiple methods or functions that describe a material's characteristics, such as the relative permeability and capillary pressures. These parameters affect the hydration or dewatering characteristics of the material and can influence aqueous transport through the material. The van Genuchten-Mualem model is used for this analysis. Table 12 shows the parameters needed to describe the relative permeability and capillary pressure of soil and grout. These values will remain the same for all simulation analysis.

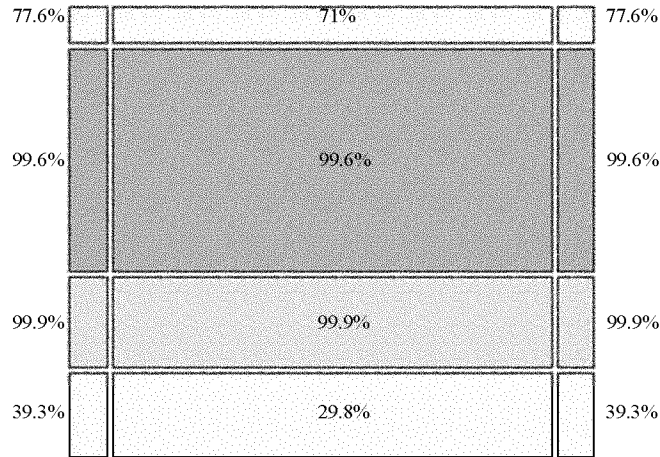


Figure 13. Steady state saturation values for the monolith.

Table 12. van Genuchten-Mualem model parameters for relative permeability and capillary pressure.

Relative Permeability	Soil	Grout
RP1 Lambda ( $\lambda$ ) (“m” van Genuchten model)	0.343	0.363
RP2 Irreducible water saturation ( $S_{ir}$ )	0.142 <sup>a</sup>	0.40 <sup>b</sup>
RP3 Liquid saturation ( $S_{ls}$ )	0.97 <sup>c</sup>	0.95 <sup>c</sup>
RP4 Saturation gas residual ( $S_{gr}$ )	0.03	0.05
Capillary pressure		
CP1 Lambda ( $\lambda$ )“m” (van Genuchten model)	0.343	0.363
CP2 Irreducible water saturation ( $S_{ir}$ )	0.138 <sup>d</sup>	0.36 <sup>d</sup>
CP3 1/Pressure ambient (“ $\alpha$ ” van Genuchten)	0.1066 m <sup>-1</sup>	7.5 × 10 <sup>-5</sup> m <sup>-1</sup>
CP4 Pressure maximum	1.e7	1.e7
CP5 Liquid saturation ( $S_{ls}$ )	1.0	1.0

a. Baca et al. (1992).

b. Graphical interpretation from capillary pressure vs. water saturation curves from Baroghel-Bouny et al. (1999).

c. Calibrated value established to ensure simulation convergence.

d. Intentionally set lower than  $S_{ir}$  as outlined in TOUGH2 User’s Guide.

The equation of state module, EOS7R, requires the user to specify the phase conditions desired for model simulation and analysis. A two-phase condition was chosen to represent the variability of saturation in the vadose zone and the monolith. Gas saturation values are included as primary variables that must be assigned to initiate two-phase conditions within material properties of the model. A generous and potentially high saturation value of 50 % was assigned to the soil encapsulating the monolith). The monolith was assigned a value of 100 % simulating the initial conditions of grout injection.

Model analysis was assumed to be isothermal with a temperature of 10.5°C. The assumption maintains that a temperature gradient will not influence contaminant transport through the monolith, and the assigned temperature closely matches subsurface values recorded at the SDA. An initial model run was used to establish an initial pressure gradient. The pressure gradient was formed through the vertical

layers of the monolith and established with reference to the atmospheric pressure at the SDA site, which was 84,700 Pa.

### 3.8.1 Solubility

The final variables to be defined for the simulation are the aqueous phase mass fractions for the parent radionuclides and daughter products. These mass fractions refer to the mass of water in the element where the contaminant will be positioned. The solubility limit of a chemical is an important consideration when modeling flow and transport of chemicals. As implied, the solubility limit restricts the total amount of chemical that can be present in the aqueous phase. Unfortunately, the EOS7R module does not provide any intrinsic constraints on radionuclide concentrations and therefore disregards chemical solubility limits (Pruess 1999). An implicit assumption of the EOS7R module is: any aqueous radionuclide concentrations are in small quantities. Some COPCs in the SDA site are in very large quantities, and modeling these quantities would produce erroneous results because the EOS7R module will ignore the chemicals solubility limits and assign proportional masses to the gaseous, aqueous and adsorbed phases. To address this issue, large quantities of COPC that exceeded their solubility limit were modeled at their solubility limit and allowed to proceed through the duration of the simulation. All the COPCs in the monolith were assumed to be in equilibrium between the mass in the aqueous and adsorbed phases with “free” product present. Two outcomes developed, based on this strategy.

1. The first outcome described COPCs with characteristically large distribution coefficients ( $K_d$ ), which retarded the transport and release of COPC from the monolith so that less than 30 % of the mass within the aqueous phase was released from the model during 10,000 years. Because it was uncertain what amount of COPCs could be available or in contact with the aqueous phase for replacing this mass loss, it was concluded that this assumption was appropriate to represent the total expected mass release from the monolith.
2. The second outcome describes COPCs with small, less than  $0.005 \text{ m}^3/\text{kg}$  distribution coefficients that have less influence on the transport and mass release from the monolith. When the mass loss from the aqueous phase was greater than 30%, the simulation was terminated. The time to reach this point was recorded and the output file of variables was reinserted into the input deck. The elements below and surrounding the source element maintained their current aqueous concentration of contaminants, but the source element was recharged with a concentration matching the chemicals solubility limit. This simulated free product transitioning into the aqueous phase. The simulation was run again until either 30 % more mass was lost from the aqueous phase, or the total free mass was deleted to zero, or if the total time of succeeding simulations exceeded 10,000 years. The duration for mass release was based on the accumulation of terminated simulations times and total mass released.

COPCs in quantities less than their solubility limit were modeled as total mass in the aqueous phase with no free product available to recharge the aqueous phase. Table 13 identifies those COPCs that were expected to exceed their respective solubility limits and those expected not to be solubility limited.

The simulations were completed until no mass remained in the model or the simulation reached 10,000 years. Daughter products were not modeled and the initial mass fraction was defined as zero for all simulations.

Table 13. Solubility and non-solubility limited contaminants of potential concern

Solubility Limited	Not Solubility Limit
U-234	Tc-99
U-235	C-140
U-235	Pb-210
U-238	U-233
Sr-90	Nitrates
R-226	Chloride 36
Pu-239	I-129
Pu-240	C-137
Methylene chloride	Nb-94
Carbon tetrachloride	Np-237
Tetrachloroethylene	Am-241
	Ac- 227

An important parameter affecting contaminant transport is infiltration. Precipitation was modeled as infiltration and included as an initial condition for each simulation analysis. Two values of infiltration were chosen representing separate conditions for the mass release analysis. A value of 0.037 cm/yr and 0.114 cm/yr were chosen to represent the presence or lack of a protective cap barrier over the grouted waste monolith, respectively. Infiltration was held constant for the simulated 10,000 years.

### 3.8.2 Soilcrete Monolith Fracturing

The causes for potential crack formation and fractures in the grout waste monolith are numerous. However, the most likely source of planar fractures within the monolith would be cold seams.<sup>b</sup> Cold seams are vertical discontinuous interfaces that develop between soilcrete columns during the injection procedure. As with most engineered projects, the structural expanse of the monolith is a progressive rather than sudden process. As rows of soilcrete columns are vertically placed, time lapses in the curing reaction between rows will cause a discontinuous interface. These interfaces are described as cold seams and depend largely on the differences in curing and shrinkage. This is especially important considering the size of an area to be jet grouted and the time required. Based on the projected number of columns that can be installed per day, the presence of cold seams would be spaced at approximately 6 m (20-ft) intervals.<sup>c</sup> The large spacing between fractures is supported from observations made of other buried cementitious vaults sites. Walton (1994) stated, “Crack width and spacing (in cementitious vaults) are a function of total shrinkage and external restraint. Without restraint (e.g. steel reinforcement), cracks tend to be large and widely spaced.”

Fracture planes in the horizontal plane were not modeled, thus, contaminant transport takes place only in the vertical direction. This conservative approach was used to direct the flow path of the contaminants from the monolith toward the underlying groundwater (Lasswell 2001).

b. Fonseca, Fernando, Professor of Civil and Environmental Engineering, Brigham Young University, Provo, UT, August, 2002, personal communication.

c. G.G. Loomis, INEEL project specialist, personal communication to Eric Miller, INEEL, August 2002.

### 3.8.3 Fracture Aperture

TOUGH2 models fractures as a continuum of the matrix block volume with the MINC method described in the Simulation Code Section. The fracture aperture is considered constant throughout the width of the fracture continuum. The fracture continuums modeled in the grout waste monolith were assigned a fixed aperture of 1 mm. As part of the Milian et al. (1997) report, researchers describe fracturing the TECT1/INEEL soilcrete specimens following wet-dry cycle testing. The cracking appeared to stabilize after eight cycles were completed. The test involved cycling the specimen 12 times, from 60°C dry to 20°C wet (ASTM Standard D-4843 1999). The TECT1/INEEL specimens had consistent fracture apertures of 1 mm.

### 3.8.4 Baseline Fracture Density

The degree of fracturing is modeled as a ratio of the fracture volume to the total volume of the mesh element of interest. For example, a 1-m<sup>3</sup> mesh element with a single fracture with an aperture of 1 cm represents 1% of total volume of the mesh element.

As discussed previously, cold seams would exist at approximately 6.1-m (20-ft) intervals between soilcrete columns. This distance serves as the baseline for fracture spacing within the monolith, creating a 6.25-m (205-ft) vertical fracture spacing along each horizontal plane for a total fracture density of 12.5. Scaling the cold seam intervals to fit the model dimensions of 8.52 m (28 ft) in horizontal x-y dimensions and maintaining an approximate fracture density of 12, the positioning of fractures was every 1.40 m (4.7 ft) in each direction. This is important visually, but conceptually TOUGH2 models fracture as a single continuum. The position of the fractures is unimportant, but defining the fractional volume is critical. Therefore, for a single fracture with an aperture of 0.1 mm, the fractional volume in reference to the 72.58 m<sup>3</sup> central element is 1.174 E-5. Multiple fractures will increase this fractional volume accordingly for numerical calculations of mass balances.

### 3.8.5 Fracture Characterization

TOUGH2 permits the user to characterize the fracture continuum with the same parameters used to characterize the material properties of the matrix, such as the porosity, permeability, and moisture content. The moisture content of the fracture was assumed to have 100 % liquid saturation similar to the corresponding grout medium where the fracture is located. The porosity of the fracture was given a value of 90 %. This value is much larger than the porosity given to the grouted medium (28 percent), but remains a conservative estimate considering that the porous nature of fractures in grout have not been readily described over an extended period. The geochemical interactions of grout and fluid can change the porous nature of the fracture over time.

The method for determining fracture permeability was obtained in part from the equation for hydraulic conductivity embedded within the cubic law used for describing flow through a fracture. The cubic law states that for a given gradient, the flow through a fracture is proportional to the cube of the fracture aperture, and is in the form:

$$Q = \frac{\rho_w g b^2}{12\mu} (bw) \frac{\partial h}{\partial L} \quad (4)$$

which resembles the commonly recognized form of Darcy's Law ( $Q=KiA$ ), where  $i$  is the gradient ( $dh/dL$ ) and  $A$  is the cross-sectional area perpendicular to flow ( $bw$ ). The hydraulic conductivity ( $K$ ) is a property of fluid and matrix properties. (Domenico and Schwartz 1990).

The properties of the matrix are described as:

$$k = \frac{b^2}{12} \quad (5)$$

where  $k$  is the permeability of the fracture, and  $b$  is the fracture aperture. With this equation, the permeability of a fracture with a 0.1mm aperture has a permeability of  $8.33 \times 10^{-10} \text{ m}^2$ . Fractures were generated internally through the MINC code of TOUGH2 and are defined within the x and y vertical planes of the GWM.

### 3.8.6 Contaminant of Potential Concern Mass Fraction Estimates

To introduce contaminant mass into the simulation, TOUGH2 requires an estimate of the ratio of the mass of each contaminant to the total mass of water in which that contaminant exists. Consequently estimates were made of (1) the total contaminant masses for each COPC and (2) the waste volume in which each COPC was originally buried from which the mass of water within that volume can be estimated. These values, along with estimates of waste zone porosity and saturation ratio, allow an estimate of the contaminant-to-water mass fractions for each COPC. Contaminant-to-water mass fractions will be used as the initial mass inputs into the predictive simulation.

Radionuclide contaminant masses were calculated based on activities referenced in Holdren et al. 2002 (Table 14) and specific activities calculated from individual radionuclide half-lives and molecular weights.

The total nitrate mass estimate was derived from summing the nitrate masses of individual nitrate-containing contaminants based on data from LMITCO (1995). The mass of nitrates from each species was estimated from the total reported mass of each species and prorated based on the ratio of the nitrate to total molecular mass for each species (Table 15).

Mass estimates of carbon tetrachloride were taken from the *Reconstructing the Past Disposal of 743-Series Waste in the Subsurface Disposal Area for Operable Unit 7-08, Organic Contamination in the Vadose Zone* report (Miller and Varvel 2001). Methylene chloride estimates were taken from *A Comprehensive Inventory of Radiological and Nonradiological Contaminants in Waste Buried in the Subsurface Disposal Area of the INEL RWMC During the Years 1952–1983* (LMITCO 1995), and tetrachloroethylene estimates were taken from *Mass Estimates of Organic Compounds Buried in the Subsurface Disposal Area for Operable Units 7-08 and 7-13/14* (Varvel 2001).

Table 16 summarizes the estimated inventories of radiological, inorganic, and volatile organic COPCs.

Table 14. Activity, half-life, and molecular weights of radiological COPCs.

Radionuclide	Best-Estimate Inventory (Ci)	<sup>a</sup> Half Life (yr)	<sup>a</sup> Molecular weight (g/g-mol)	<sup>b</sup> Specific Activity (Ci/g)
Ac-227	5.12E-07	21.77	227.03	7.24E+01
Am-241	1.83E+05	432.2	241.06	3.43E+00
C-14	5.00E+02	5715	14.00	4.47E+00
Cl-36	1.11E+00	3.01E+05	35.97	3.30E-02
Cs-137	6.17E+05	30.3	136.91	8.62E+01
I-129	1.58E-01	1.7E+07	128.90	1.63E-04
Nb-94	1.00E+03	2.4E+04	93.91	1.59E-01
Np-237	2.64E+00	2.14E+06	237.05	7.05E-04
Pa-231	8.64E-04	3.25E+04	231.04	4.76E-02
Pb-210	5.10E-07	22.6	209.98	7.54E+01
Pu-239	6.49E+04	2.41E+04	239.05	6.21E-02
Pu-240	1.71E+04	6537	240.05	2.28E-01
Ra-226	6.00E+01	1599	226.03	9.90E-01
Sr-90	6.44E+05	29.1	89.91	1.37E+02
Tc-99	6.05E+01	2.13E+05	98.91	1.70E-02
U-233	1.51E+00	1.59E+05	233.04	9.66E-03
U-234	6.74E+01	2.45E+05	234.04	6.24E-03
U-235	5.54E+00	7.04E+08	235.04	2.16E-06
U-236	2.86E+00	2.34E+07	236.05	6.48E-05
U-238	1.17E+02	4.46E+09	238.05	3.37E-07

a. Lide et al.

b. Specific activities calculated from radionuclide half-lives and molecular weights (i.e.,  $3.575E+05/[\text{half life (yr)} \times \text{molecular weight}]$ ).

Table 15. Nitrate-containing chemicals in Subsurface Disposal Area waste and total estimated nitrate inventory.

Nitrate Containing Species	Molecular Formula	Molecular Weight (g/g-mol)	Total Mass (kg)	Nitrate Mass (kg)
Aluminum nitrate nonahydrate	Al(NO <sub>3</sub> ) <sub>3</sub> 9H <sub>2</sub> O	375.13	1.9E+05	9.42E+04
Copper nitrate	Cu(NO <sub>3</sub> ) <sub>2</sub>	187.56	3.3E-01	2.2E-01
Mercury nitrate monohydrate	Hg(NO <sub>3</sub> ) <sub>2</sub> H <sub>2</sub> O	342.64	8.1E+02	2.93E+02
Potassium nitrate	KNO <sub>3</sub>	101.1	1.8E+06	1.10E+06
Sodium nitrate	NaNO <sub>3</sub>	84.99	1.2E+06	8.76E+05
Uranyl nitrate	UO <sub>2</sub> (NO <sub>3</sub> ) <sub>2</sub>	394.02	2.2E+02	6.92E+01
Total				2.07E+06

Table 16. Estimated inventory of contaminants of potential concern in Subsurface Disposal Area waste.

Category	Contaminant of Potential Concern	Total Estimated Mass (kg)
Radionuclides	Ac-227	7.07E-12
	Am-241	5.33E+01
	C-14	1.12E-01
	Cl-36	3.36E-02
	Cs-137	7.15E+00
	I-129	9.68E-01
	Nb-94	6.30E+00
	Np-237	3.74E+00
	Pa-231	1.81E-05
	Pb-210	6.77E-12
	Pu-239	1.05E+03
	Pu-240	7.50E+01
	Ra-226	6.06E-02
	Sr-90	4.71E+00
	Tc-99	3.56E+00
	U-233	1.56E-01
	U-234	1.08E+01
U-235	2.56E+03	
U-236	4.42E+01	
U-238	3.47E+05	
Inorganics	Nitrates	2.07E+06
Volatile organic compounds	Carbon tetrachloride	8.20E+05
	Methylene chloride	1.40E+04
	Tetrachloroethylene	9.80E+04

Following the estimate of the total contaminant masses for each COPC, estimates were made of the waste volume in which each COPC was buried. The WasteOScope database was queried and specific waste zone areas for 15 of the 24 COPCs were determined. Waste areas for the remaining 9 COPCs were not available. For these nine COPCs, a waste area of 300 m<sup>2</sup> was assumed to approximate the waste area of the Cl-36 (the smallest waste area reported from WasteOScope). Using these values, and an estimated waste zone thickness of 3 m, waste zone volumes were calculated for each COPC. From these waste zone volumes, water volumes were calculated assuming a waste zone porosity of 0.6 (Loomis et al. 2002) and a water saturation ratio of 0.30. The water saturation ratio of 0.30 is based on surface soil parameters from the SDA and are assumed to be conservative in that they are based on the irreducible water content of surficial soils (i.e., 0.142) at a porosity of 0.487 (Baca et al., 1992). The resulting estimates of water mass, along with estimates of waste zone areas, and waste zone volumes for each COPC, are found in Table 17.

Table 17. Estimated waste zone areas, waste zone volumes, and water mass for each COPC.

Category	Contaminant of Potential Concern	<sup>a</sup> Estimated Waste Zone Area (m <sup>2</sup> )	<sup>b</sup> Estimated Waste Zone Volume (m <sup>3</sup> )	<sup>c</sup> Estimated Water Mass (kg) in Waste Zone
Radionuclides				
	Ac-227	300	900	1.62E+05
	Am-241	61,837	185,511	3.34E+07
	C-14	2,563	7,689	1.38E+06
	Cl-36	336	1,008	1.81E+05
	Cs-137	300	900	1.62E+05
	I-129	555	1,665	3.00E+05
	Nb-94	3,023	9,069	1.63E+06
	Np-237	1,306	3,918	7.05E+05
	Pa-231	300	900	1.62E+05
	Pb-210	300	900	1.62E+05
	Pu-239	300	900	1.62E+05
	Pu-240	300	900	1.62E+05
	Ra-226	300	900	1.62E+05
	Sr-90	300	900	1.62E+05
	Tc-99	564	1,692	3.05E+05
	U-233	10,409	31,227	5.62E+06
	U-234	10,409	31,227	5.62E+06
	U-235	10,409	31,227	5.62E+06
	U-236	10,409	31,227	5.62E+06
	U-238	10,409	31,227	5.62E+06
Inorganics				
	Nitrates	15,461	46,383	8.35E+06
Volatile organic compounds				
	Carbon tetrachloride	32,775	98,325	1.77E+07
	Methylene chloride	300	900	1.62E+05
	Tetrachloroethylene	32,775	98,325	1.77E+07

a. Burial areas obtained from WasteOScope database (except where burial area data from WasteOScope was not available; for these radionuclides an area of 300m<sup>2</sup> was arbitrarily chosen to be approximately equal to the smallest reported area of 336 m<sup>2</sup> for Cl-36).

b. Assumes a waste zone thickness of 10 ft (3 m)

c. Assumes a waste zone porosity of 0.6, and water saturation ratio of 0.3, and a water density of 1000 kg/m<sup>3</sup>

By dividing the total contaminant mass (Table 16) by the total mass of water in which that contaminant exists (Table 17), an individual contaminant to water unit mass fraction was estimated for each COPC (Table 18).

Table 18. Estimated contaminant of potential concern mass fractions.

Category	Contaminant of Potential Concern	Mass Fraction (kg <sub>COPC</sub> /kg <sub>water</sub> )
Radionuclides		
	Ac-227	4.36E-17
	Am-241	1.60E-06
	C-14	8.12E-08
	Cl-36	1.86E-07
	Cs-137	4.41E-05
	I-129	3.23E-06
	Nb-94	3.87E-06
	Np-237	5.30E-06
	Pa-231	1.12E-10
	Pb-210	4.18E-17
	Pu-239	6.48E-03
	Pu-240	4.63E-04
	Ra-226	3.74E-07
	Sr-90	2.91E-05
	Tc-99	1.17E-05
	U-233	2.78E-08
	U-234	1.92E-06
	U-235	4.56E-04
	U-236	7.86E-06
	U-238	6.17E-02
Inorganics		
	Nitrates	2.48E-01
Volatile organic compounds		
	Carbon tetrachloride	4.63E-02
	Methylene chloride	8.64E-02
	Tetrachloroethylene	5.54E-03

Using these mass fractions and the mass of water calculated from the volume of the modeled waste grid block, contaminant masses were loaded as initial mass inputs into the predictive simulation.

## 3.9 Base Case Results

### 3.9.1 Estimating Mass Release from the Grout Waste Monolith

As mentioned previously, TOUGH2 has limited capabilities for modeling aqueous phase equilibrium because it does not consider a chemical's solubility limit. To work around this limitation, the total mass of water available and the chemical's solubility limit were needed to calculate the mass of contaminant to be loaded into the model, so the theoretical maximum aqueous phase concentration would not be exceeded. Because some COPCs are in quantities greater than can be sustained at one time in the aqueous phase, the user must interrupt the simulation when the mass in the aqueous phase has been depleted, and reload the model with the remaining mass. This approach was used to estimate the mass released for each COPC from the monolith. Mass release analysis of the COPCs were separated into five groups or categories based on the mass present of each COPC and its solubility limit. Solubility limits estimated for each COPC at pH of 10.5 and Eh of 310 mV (Table 7) were used to support mass loading.

Group 1 includes COPCs that are present in low enough amounts and have sufficiently high solubility limits that they can be completely dissolved in the aqueous phase of the model without reaching the solubility limit. Tc-99, C-14, Pb-210, U-233 and nitrates were in this grouping. Three other radionuclides with unknown solubility limits, Cl-36, I-129, and Cs-137, were also included in Group 1. It was assumed that each of these elements would be entirely in the aqueous phase. This may be oversimplified; however, because this would represent the worst-case scenario for studying release of these radionuclides from the monolith. The entire mass of the COPCs of interest was loaded into the aqueous phase and TOUGH2 partitioned the mass among the phases. The simulation proceeded to 10,000 years with no alterations.

The second grouping of COPCs, Group 2, were made up of the uranium species, 234, 235, 236, and 238. The solubility limit for each uranium species is identical and very small ( $3.32\text{E-}4$  mg/L). This restricts the total mass that can be present in the aqueous phase. Subsequently, only 674 mg of uranium are ever present in the aqueous phase of the model. This mass is considerably less than the amount of any uranium species present in the SDA. These radionuclides have identical grout distribution coefficients ( $K_d$  of  $1.0$  m<sup>3</sup>/kg) and half-lives greater than  $2.50\text{E-}5$  years. Because this mass present in the aqueous is small on an absolute scale, concentration gradients are also small and, along with a  $K_d$  of  $1.0$  m<sup>3</sup>/kg, contaminant transport will be retarded. The amount of mass released from the aqueous phase is less than 5 % during 10,000 years. For this reason, the aqueous phase is considered saturated through the simulation and no adjustments are necessary to model the remaining mass of uranium present.

Group 3 contained radionuclides whose mass was greater than the amount that could be dissolved in the aqueous phase, but were expected to be more than the 10% depleted from their initial aqueous phase mass within 10,000 years. These included radionuclides Sr-90, Ra-226, Pu-239 and Pu-240. It is assumed that the mass of these compounds initially present is large enough to continue to be a source dissolving into the monolith's aqueous phase. When the mass in the aqueous phase of the source element was depleted by 10%, the simulation was stopped. The time to reach this point was noted and subtracted from 10,000 years to obtain a total run time for mass released. The simulation was restarted with concentrations in the matrix at the time the simulation was stopped, however, the source element was changed back to its original concentration. The simulation proceeded until the source element was again depleted by 10% or until the total run time of 10,000 years was expired. This procedure simulated a maximum concentration in the aqueous phase through the duration. Half-lives and initial masses present

were checked to ensure that there would always be a mass source available to maintain a saturated condition.

**Note:** Sr-90 could not be modeled effectively because of its low solubility and its short half-life (29 years). Similarly, Ra-226 could not be modeled with accuracy. The half-life is 1,600 years but the limited solubility makes it difficult to model within the constraints of TOUGH2. Degradation through decay makes it difficult to anticipate the mass remaining in the source block for further aqueous phase replenishment. These chemicals were left blank in Table 14. Nonetheless, mass release curves were generated at their respective solubility limits to note trends in the mass release curve.

Group 4 was made up of COPCs difficult to accurately model with their associated parameters. Nb-94 and Np-237 have very small masses initially present in the aqueous phase because of their low solubility limits. TOUGH2 was not able to perform the necessary computations correctly with these small masses because adequate precision in the calculations was lacking. Am-241 and Ac-227 were also included in Group 4 because of the small mass initially present in the aqueous phase and their short half-lives of 423 and 22 years, respectively. These factors make it difficult to perform the same procedure as in Group 3 for tracking mass release, because decay occurs rapidly with the small masses present. Subsequently, Group 4 COPCs were modeled for the total mass present at the SDA without regard to the solubility limit, to obtain a worst-case scenario for mass release.

The final grouping, Group 5, was made up of the VOCs, methylene chloride, carbon tetrachloride, and tetrachloroethylene. Presumably, these compounds do not adsorb to grout and thus have zero  $K_d$ 's. These compounds are transported through a two-phase system of liquid and gas flow. The initial mass was loaded into the aqueous phase according to the respective solubility limits of the COPCs. An interval for the mass released was estimated by determining a transport rate for 10% depletion of mass. It was assumed that VOCs transport is continuous and the source mass will replenish the maximum concentration in the aqueous phase until no source remains.

### **3.9.2 Estimation of the Mass of Contaminants of Potential Concern Released from Monolith over 10,000 Years**

Table 19 shows the percentage and mass of COPC that was released from the monolith, and the time it took for this amount to be released. Some chemicals were completely released from the monolith before the 10,000-year simulation was completed. All results were modeled with an engineered cover or cap producing an infiltration rate of 0.037 cm/yr with no fractures.

As expected, Tc-99 and the nitrates were released from the monolith in the shortest time, 100 and 500 years, respectively. This is because both COPCs have a grout distribution coefficient ( $K_d$ ) of zero, and therefore, the aqueous mass transport is not retarded through the monolith. Figure 14 shows how quickly mass is released from the monolith when no distribution coefficient is associated with the chemical. Nitrate had over 400% more mass in the aqueous phase than TC-99, requiring more time for complete release.

Table 19. Contaminant of potential concern mass released from grout waste monolith during 10,000 years.

COPC	Percent Released	Mass Released	Time of Release	Grout $K_d$	T 1/2
<b>Group 1</b>	(%)	(kg)	(yrs)	(m <sup>3</sup> /kg)	(yrs)
Tc-99	100.00%	38.99	100	0.000	213,000
Nitrates	100.00%	16342	500	0.000	0.0
Cs-137	100.00%	38.69	2,000	0.020	30.2
Pb-210	100.00%	5.7E-4 (mg)	3,000	0.500	22.3
Ch-36	100.00%	0.143	4,000	0.001	301,500
I-129	100.00%	2.312	9,000	0.005	1.57E+07
C-14	71.00%	1.43	10,000	0.100	5730
U-233	3.78%	8.14E-04	10,000	1.000	1.59E+05
<b>Group 2</b>					
U-234	< 0.1%	1.52E-03	10,000	1.000	2.46E+05
U-235	< 0.01%	4.60E-04	10,000	1.000	7.04E+08
U-236	< 0.01%	6.36E-04	10,000	1.000	2.34E+07
U-238	< 0.01%	8.27E-04	10,000	1.000	4.47E+09
<b>Group 3</b>					
Sr-90	—	—	—	0.001	2.91E+01
Ra-226	—	—	—	0.050	1.60E+03
Pu-239	< 0.01%	0.070	10,000	5.000	2.41E+04
Pu-240	< 0.1%	0.155	10,000	5.000	6.56E+03
<b>Group 4</b>					
Ac-227	100.00%	0.022	500	1.000	2.18E+01
Am-241	100.00%	1.24	8,000	1.000	4.33E+02
Nb-94	30.37%	0.761	10,000	1.000	2.00E+04
Np-237	1.22%	0.05	10,000	2.000	2.14E+06
<b>Group 5</b>					
Methylene Chloride	100.00%	67,742.0	5,930	0.000	0.0
Carbon Tetrachloride	11.38%	4,134.0	10,000	0.000	0.0
Tetrachloroethylene	17.07%	741.0	10,000	0.000	0.0

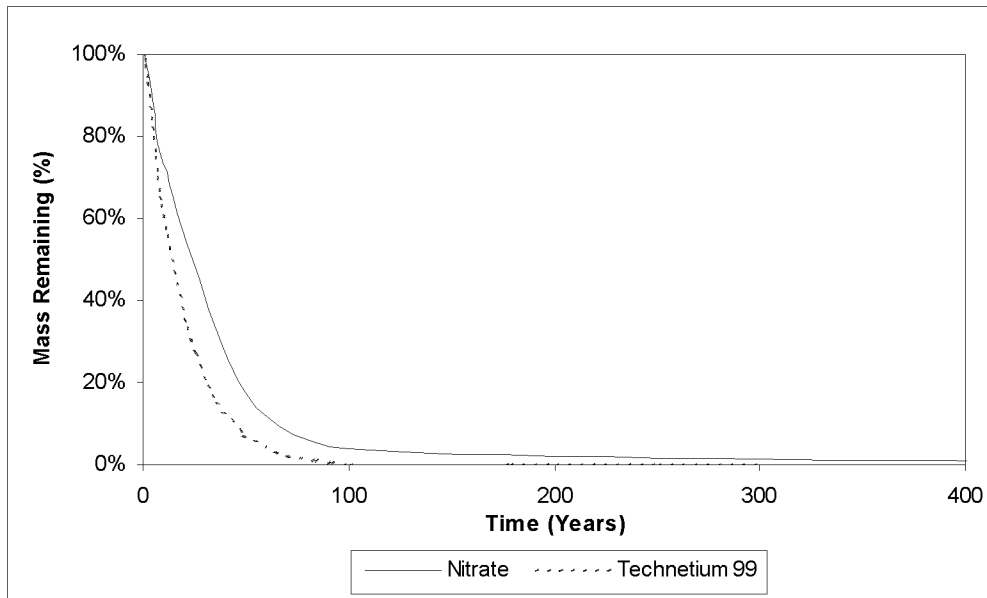


Figure 14. Mass remaining curves of chemicals with no associative  $K_d$ .

Within Group 1, four other chemicals with  $K_d$ 's (I-129, Pb-210, Cs-137, and C-136) were released completely from the grouted waste monolith within 10,000 years. This can be attributed to a combination of factors. Each of these COPCs have grout distribution coefficients less than  $0.5 \text{ m}^3/\text{kg}$ , small initial masses, and, in the case of Pb-210 and Cs-137, short half-lives (22.3 and 30.2 years, respectively) which contribute to mass loss through decay. Figure 15 shows how significant half-life contributes to mass released or lost with respect to Cl-36 and I-129 (see Table 19). Carbon-14 was not completely released or depleted from the monolith primarily because of a larger  $K_d$  of  $0.1 \text{ m}^3/\text{kg}$  and a longer half-life of 5,730 years (see Table 20).

Elements with a  $K_d$  of  $1.0 \text{ m}^3/\text{kg}$  or greater as seen in Groups 2 and 3 are less likely to escape from the monolith in quantities greater than 0.001 kg. An important caveat to the limited release is the initial mass in the aqueous phase. Extremely small mass in the aqueous phase reduces the effects of the concentration gradients on COPC transport through the monolith. The COPCs uranium and plutonium have low solubility limits (uranium,  $3.32 \text{ E-4 mg/L}$ , plutonium,  $4.23 \text{ E-4 mg/L}$ ) and thus impart a limited total mass in the aqueous phase (uranium, 674 mg, plutonium, 859 mg). Although plutonium, with a grout  $K_d$  of  $5.0 \text{ m}^3/\text{kg}$ , shows more mass released than any uranium species ( $K_d$  of  $1.0 \text{ m}^3/\text{kg}$ ), plutonium's half-life is two orders of magnitude shorter than any uranium species, and therefore, loss is attributed to depletion rather than transport (see Table 19). Figure 16 shows the relationship of half-lives and  $K_d$ 's contributing to mass release or lost from the grout waste monolith.

Sr-90 and Ra-226 have a combination of factors influencing their mass loss. These COPCs have  $K_d$ 's less than  $0.05 \text{ m}^3/\text{kg}$ , short half-lives, and small masses initially present. These factors contribute to the complete release from the monolith within 10,000 years. Characteristic mass release curves for these elements are similar to Figure 16 and appear in Appendix A, but represent a single mass loaded at the solubility limit and not the entire quantity.

Group 4 elements, Ac-227 and Am-241, were completely released from the monolith in 500 and 8,000 years, respectively. Because both COPCs have a high  $K_d$  for grout,  $1.0 \text{ m}^3/\text{kg}$ , the major contributor to mass loss is attributed to decay rather than physical transport. Ac-227 has a half-life of 22 years and Am-241 has a half-life of 433 years (see Table 19). Coupled with so little Ac-227 in the aqueous phase, 0.022 kg, compared to 1.24kg of Am-241, it is expected that Ac-227 would be depleted sooner than Am-241 (see Figure 17).

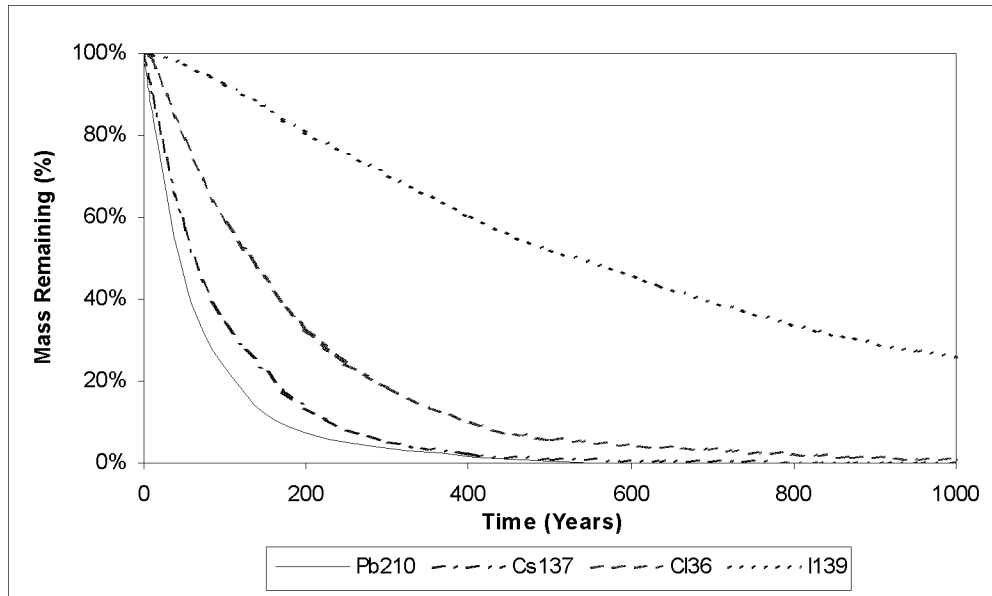


Figure 15. Mass remaining curves of chemicals with increasing no associative  $K_d$ .

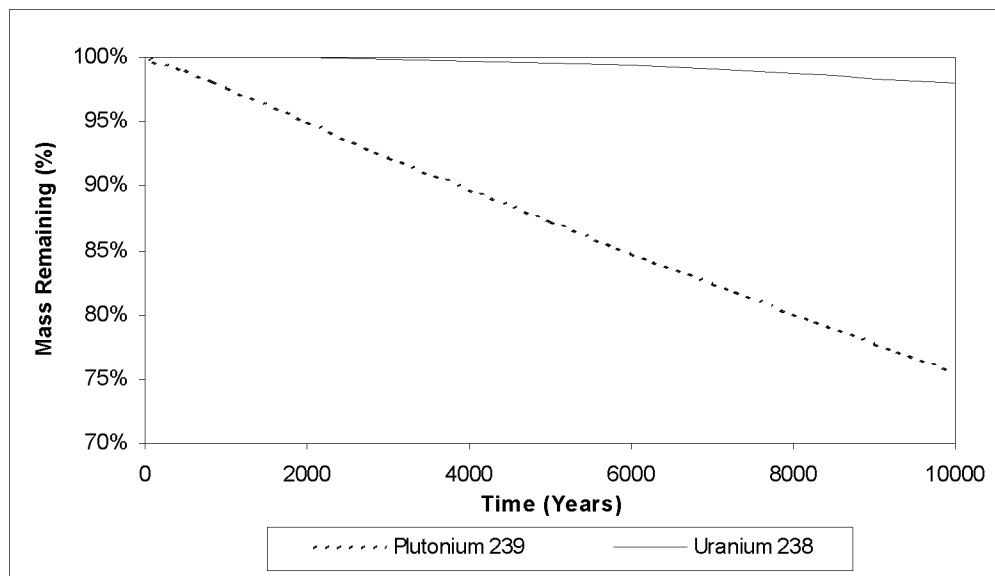


Figure 16. Mass remaining curves of U-238 and Pu-239.

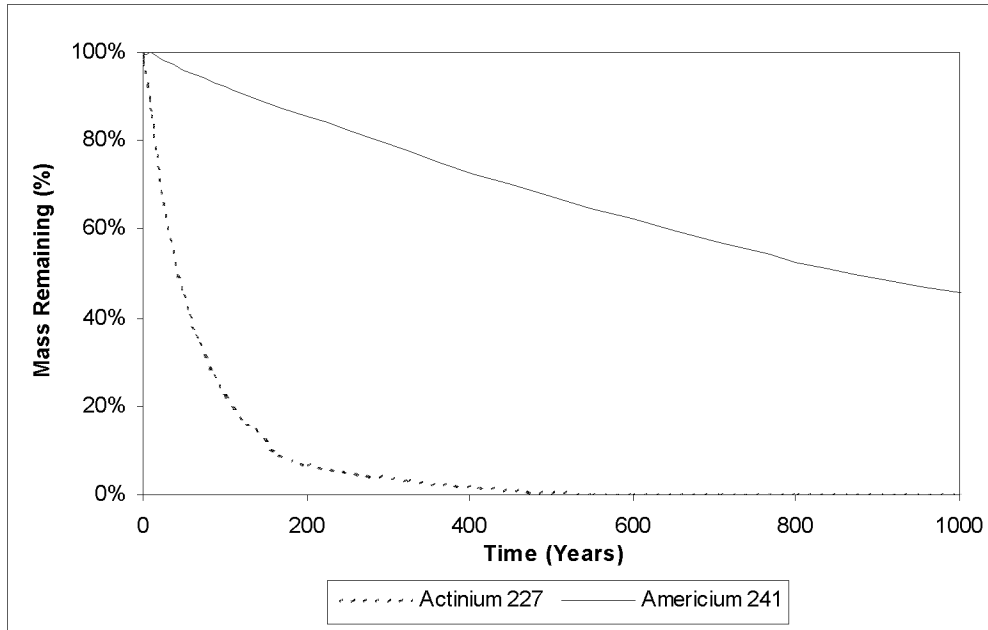


Figure 17. Mass remaining curve of Ac-227 and Am-241.

Only 30.4% of Nb-94 and 1.2% of Np-237 were released within 10,000 years. The half-lives of both of these COPCs are greater than 10,000 years (Nb-94, 20,000 years and Np-237, 2,140,000 years). Therefore, the loss of mass is attributed to transport, which is slowed by a relatively high adsorption or distribution coefficient ( $K_d$ ) for grout (Nb-94 is  $1.0 \text{ m}^3/\text{kg}$  and Np-237 is  $2.0 \text{ m}^3/\text{kg}$ ).

Volatile organic compounds in Group 5 are dependant on liquid and gas phase equilibriums for transport not on adsorptive characteristics. Methylene chloride was completely released from the monolith in 5,930 years, whereas carbon tetrachloride and tetrachloroethylene remained in the monolith after 10,000 years. The solubility limit of methylene chloride is  $2.37 \text{ E-4 mg/L}$ , which means, 483.3 kg are dissolved in the aqueous phase of the matrix. Carbon tetrachloride and tetrachloroethylene have solubility limits that are smaller, only 17.0 kg and 3.0 kg, respectively, therefore, are soluble in the aqueous phase of the matrix. The large mass of methylene chloride diffusing into the aqueous phase permits more mass to be transported from the monolith over time. Curves describing mass release for VOCs are in Appendix A and are similar to curves generated for Tc-99 and nitrate (see Figure 15). However, the curves represent a single mass loaded at the solubility limit and do not represent the entire quantity of mass buried at the SDA.

Appendix A contains tables and graphs of the characteristic mass release curves of the COPCs from the grouted waste monolith under three conditions (1) an engineered cover or cap, (2) no cover, and (3) with a cover and a fracture density of 6.25 fractures.

### 3.10 Sensitivity Cases

#### 3.10.1 Grid Discretization Density

The finite difference method used by TOUGH2 allows flexibility for solving system equations in regular and irregular space discretizations of 1D, 2D and 3D. System equations, such as ones describing discretized flux, is expressed in averages between volume elements. As the volume is discretized into large or smaller elements, the size and total number of elements potentially will affect accuracy of results.

To determine how moisture content through the model is affected by increased grid resolution, a comparison between the original grid size and three different configurations of increased resolution were analyzed. The newly configured grids were constructed as follows:

- Horizontal resolution: Required increasing the number of rows in the x-y plane by four elements and leaving the vertical plane unchanged. Therefore, the mesh construct is four elements  $\times$  four elements  $\times$  four layers (8.5 m [28 ft]  $\times$  8.5 m [28 ft]  $\times$  four layers).
- Vertical resolution: Required increasing the number of layers in the z plane by 16 and leaving the horizontal plane (x-y) unchanged. Therefore, the mesh construct is one element  $\times$  one element  $\times$  16 layers (8.5 m [28 ft]  $\times$  8.5 m [28 ft]  $\times$  16 layers). All layers were not equal in depth but each layer was separated into four equally sized elements of the total depth of the layer. If the layer was 2 m (0.7 ft) in depth, four elements of .05 m (0.16 ft) in depth were created.
- Horizontal and vertical resolution: Required increasing the number of rows in the x-y plane by four elements and increasing the number of layers by 16. Therefore, the mesh construct is four elements  $\times$  four elements  $\times$  16 layers (2.125 m [7 ft]  $\times$  2.125 m [7 ft]  $\times$  16 layers).

Table 20 shows how the moisture content of the model changed with variations in configurations of grid refinement.

Table 20. Grout waste model moisture content.

x-y-z	Initial Volume (m <sup>3</sup> )	Final Volume (m <sup>3</sup> )
GWM coarse (1 $\times$ 1 $\times$ 4)	39.1595	37.3747
Horizontal resolution (4 $\times$ 4 $\times$ 4)	39.1589	37.2275
Vertical resolution (1 $\times$ 1 $\times$ 16)	39.1572	34.2675
Horizontal and vertical (4 $\times$ 4 $\times$ 16)	39.1672	35.3396

The horizontal resolution showed little or no change in the moisture content, whereas the vertical resolution indicated approximately 8% less water remained in the model at the end of the simulation. Combining grid refinement in both the vertical and horizontal plane showed that approximately 5% less water was retained at the end. Decreasing the element volumes and increasing the number of elements within the mesh contributes proportionately to computational efficiency, so the combined configuration leads to more reasonably accepted results. Nonetheless, having performed a moisture content comparison and determined that the difference is approximately 5% with a combined grid refinement, the original mesh design is not so inappropriate that it needs to be rejected.

In addition to sensitivity of water flow to grid resolution, the sensitivity of contaminant mass transport to increasing resolution was also evaluated. Once again, a similar analysis and comparison was made with grid refinement and the total mass of contaminant remaining within the monolith. A series of analyses were performed by doubling the resolution of the monolith grid in successive simulations for the horizontal and vertical planes. In Table 21, only the horizontal plane underwent increased grid resolution by doubling the number of rows in the x-y plane.

Table 21. Mass remaining of Tc- 99 as increased resolution in the horizontal.

Horizontal Grid Refinement				
Years	Mass Remaining kg			
	1 × 1 × 4	2 × 2 × 4	4 × 4 × 4	8 × 8 × 4
0	38.804	38.799	38.808	38.773
5	33.635	32.498	31.243	31.471
15	22.854	20.666	18.833	19.676
25	15.556	13.165	11.576	12.643
50	6.215	4.494	3.842	4.641
75	2.781	1.782	1.539	1.989
100	1.391	0.814	0.715	0.967
150	0.464	0.241	0.218	0.312

Dimensions are for x-y-z respectively.

As expected, an increase in resolution in the horizontal plane showed a decrease over time in the mass remaining from the monolith. However, it appears a threshold exists where mass remaining decreased as resolution increased from the 4 × 4 × 4 design to 8 × 8 × 4. Figure 18 shows this trend in the data. An immediate decrease occurs in the mass remaining as resolution increases from 2 × 2 × 4 to 4 × 4 × 4, but any further increase causes the results to move toward the curve of 2 × 2 × 4. Quantifiable differences in mass are observed as resolution increases. However, the differences in the times for complete release of mass for each case were considered, making grid refinement in the horizontal plane insignificant (see Table 21).

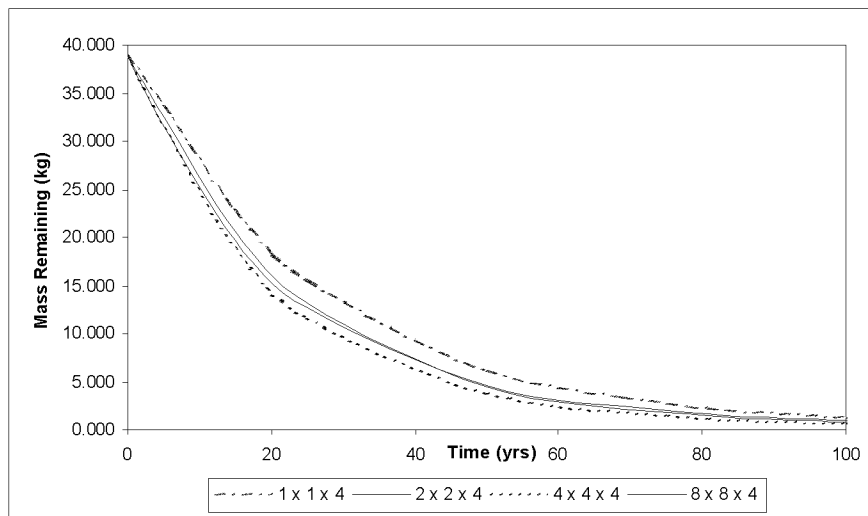


Figure 18. Grid refinement (horizontal) and mass (Tc-99) remaining in monolith.

Increasing grid resolution in the vertical plane indicated there is little change in mass remaining from the monolith over time, as the first two columns of Table 22 show. Vertical resolution alone does not alter the total amount of mass remaining in the monolith over time. Combining resolution in the vertical and horizontal planes does cause a decrease in the mass remaining, as the left column of Table 22 shows. However, the amount remaining is greater than results obtained for the 4 × 4 × 4 and 8 × 8 × 4 design.

Table 22. Mass release subject to vertical and horizontal grid refinement.

Grid Refinement: Vertical & Vertical/Horizontal					
x-y-z	Mass Remaining (kg)				
Years	1 × 1 × 4	1 × 1 × 16	4 × 4 × 4	8 × 8 × 4	4 × 4 × 16
0	38.804	38.799	38.808	38.773	38.808
5	33.635	33.154	31.243	31.471	32.159
15	22.854	22.489	18.833	19.676	20.498
25	15.556	15.350	11.576	12.643	13.248
50	6.215	6.140	3.842	4.641	4.782
75	2.781	2.795	1.539	1.989	2.000
100	1.391	1.378	0.715	0.967	0.954
150	0.464	0.461	0.218	0.312	0.300

As shown in the moisture content analysis and the mass release analysis for separate resolutions of the horizontal and vertical planes, a threshold level of mass remaining is breached and the combination of resolution in both planes would be more acceptable. Selected data from Tables 21 and 22 show how the combination of grid refinement in both planes compares to separate resolutions (see Figure 19). Note that the combined resolution moves closer to the data in the original design.

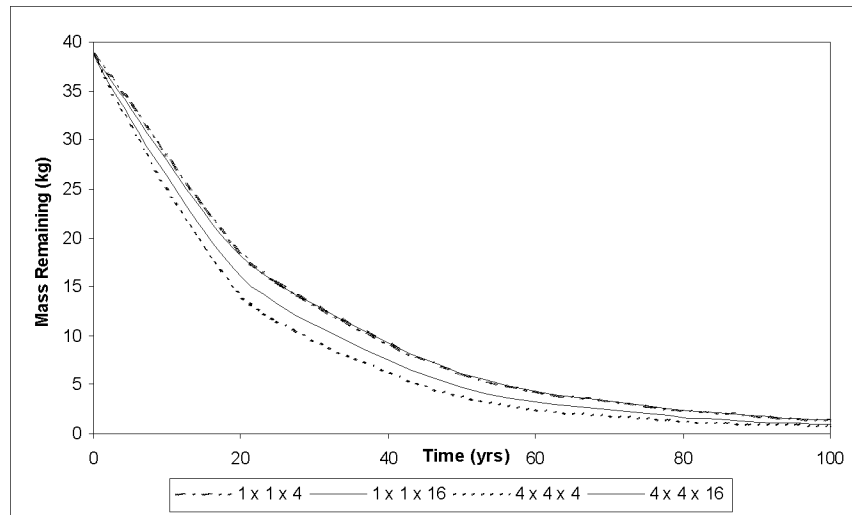


Figure 19. Grid refinement (vertical) and mass (Tc-99) remaining in monolith.

Although Figure 19 does not show the time for complete release of contaminant from the analysis, data from Table 17 indicated that no significant difference was observed among the analyses. Grid resolution is an important parameter for obtaining accurate results, however, because of uncertainty in the number of variables affecting the model and the 10,000 years desired for immobilization of COPCs, resolution did not affect the results so significantly that results obtained in this report would be disregarded.

### 3.10.2 Variability of Model Parameters

Sensitivity analysis also was performed by varying physical and hydraulic properties of the monolith to determine model variability with respect to contaminants of principle concern. Properties such as porosity, permeability and infiltration equally affect the transportability of any COPC in the aqueous phase. However, the distribution coefficient ( $K_d$ ) and half-lives of each COPC affects transport and release from the monolith. To illustrate how the physical and hydraulic properties affect transport without interference from the chemical's characteristics, the distribution coefficient and half-life were removed from computations in the analysis. This was done by creating a 'generic' radionuclide (GenRad) possessing a large half-life (1E+50 sec), and with a distribution coefficient of 0.0 m<sup>3</sup>/kg. GenRad imparted a baseline effect on contaminant transport when studying effects of the physical and hydraulic properties of grout. A separate analysis will show the affects the distribution coefficient has on contaminant mass release through transport without the influence of half-lives. A half-life sensitivity analysis was completed to illustrate how significant radioactive decay contributes to the overall mass loss of COPC through depletion, at which point inferences can be made of how much radionuclide will be released based on contributing factors for mass loss, half-life and  $K_d$ .

Mass loading in the aqueous phase is determined by porosity of the medium, and saturation level of pore spaces. A 100% liquid saturation was assumed for the pore spaces available in the monolith. This allowed for the highest potential for mass loading in the aqueous phase for mass release. Because TOUGH2 constrains the modeling of total mass at the solubility limits of the COPCs, mass loading must always be adjusted to changes in porosity to maintain the desired initial mass (solubility limit) within the aqueous phase. Therefore, performing a sensitivity analysis of porosity is a redundant exercise. The mass released over time will not change, because the same concentration is being released regardless to changes in porosity.

**3.10.2.1 Sensitivity to Permeability.** Transport of pore water throughout the monolith is critical in assessing the quantity of contaminant release. Fluid transport is described by the hydraulic conductivity of the medium and is often termed permeability. TOUGH2 addresses hydraulic conductivity or permeability as absolute permeability. The average or normal absolute permeability value chosen to represent the grout waste monolith is 3.96E-17 m<sup>2</sup>. To assess the sensitivity of the model results, the absolute permeability was increased and decreased by an order of magnitude. Thus the value of 3.96E-16 m<sup>2</sup> represents the highest end of fluid flow through the medium and is termed high permeability. Conversely, a value of 3.96E-18 m<sup>2</sup> represents the lowest end, and is termed low permeability.

Figure 20 shows the differences in the amount of mass released because of changes in permeability of the grout medium.

Increasing permeability by an order of magnitude to 10<sup>-16</sup> m<sup>2</sup> increases the amount of mass released. However, this change is small, approximately 2 % through each time point between 15 and 100 years (see Table 23). The amount of mass released when decreasing the permeability to 10<sup>-18</sup> m<sup>2</sup> produces little change. The time for complete mass depletion from the monolith remains unchanged for all three permeability values.

Variations in permeability do not significantly change the total time required for complete depletion of COPCs from the grout/waste medium.

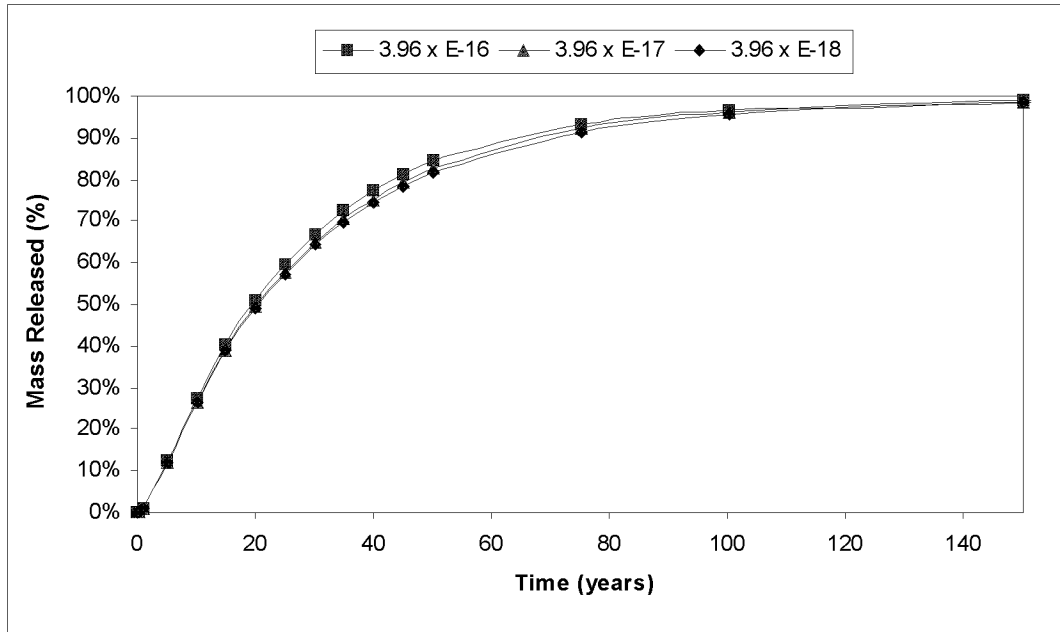


Figure 20. Mass released of GenRad because of variation in grout permeability.

Table 23. Percentage of mass released of GenRad with varying permeabilities

Time years	Perm $10^{-16}$	Mass Released	
		Perm $10^{-17}$	Perm $10^{-18}$
0.00	0.00%	0.00%	0.00%
0.25	0.06%	0.06%	0.05%
0.50	24%	22%	21%
1.00	91%	89%	88%
5.00	12.49%	12.19%	12.15%
10.01	27.36%	26.54%	26.60%
15.02	40.23%	38.90%	38.88%
20.02	51.08%	49.31%	49.17%
25.02	59.76%	57.71%	57.43%
30.02	67.00%	64.78%	64.37%
35.02	72.71%	70.46%	69.93%
40.02	77.44%	75.23%	74.59%
45.02	81.35%	79.23%	78.51%
50.03	84.58%	82.59%	81.81%
75.03	93.33%	92.07%	91.35%
100.07	96.74%	95.98%	95.48%
150.07	98.95%	98.64%	98.41%
200.32	99.66%	99.54%	99.44%
250.32	99.89%	99.84%	99.80%

**3.10.2.2 Sensitivity to Infiltration.** Fluid flow is influenced by the amount of precipitation received by the monolith. By increasing the precipitation or infiltration the monolith receives, the transport of contaminant increases via the aqueous phase. The sensitivity analysis of infiltration was studied in three configurations. The first configuration allows for an infiltrating value of 0.037 cm/yr, representing a

constructed engineered cover over the grout waste monolith. This value is the lowest. The second configuration represents the grout waste monolith left in a natural state with no cap or cover, receiving the expected rainfall as infiltration. This value is 0.114 cm/yr. The highest value for the sensitivity analysis is 0.185 cm/yr and serves as the high bounding value.

Modeling runs for these three infiltration rates showed no difference in amount of mass released or the time for complete release. To confirm that this result is not a modeling error, an arbitrary value of ten times the infiltration of 0.185 cm/yr, or 1.85 cm/yr, was run through the model. This value decreased the time for complete release of mass to be within 50 years, as opposed to 100 years for the infiltration value of 0.185 cm/yr (see Table 24). Subsequently, infiltration in the form of precipitation has no effect on COPC mass release because of the relatively low assigned permeability of the monolith.

Table 24. Mass release from infiltration values of 0.185 and 1.85 cm/yr.

Time years	Mass Release	
	0.185 cm/yr	1.85 cm/yr
0.0	0.00%	0.00%
0.5	0.70%	0.70%
1.0	2.22%	2.23%
5.0	19.94%	24.92%
10.0	38.28%	50.93%
25.0	72.13%	86.43%
50.0	92.24%	98.27%
100.1	98.92%	99.89%
200.3	99.93%	100.00%
250.3	99.98%	100.00%
300.3	100.00%	100.00%

**3.10.2.3 Sensitivity to Distribution Coefficient.** The most significant property influencing contaminants released from the monolith is the distribution coefficient ( $K_d$ ). This chemical property affects the equilibrium between aqueous phase solubility and solid phase adsorption. TOUGH2 models the distribution coefficient in units of volume of aqueous phase ( $m^3$ ) per mass (kg) of soil. A  $K_d$  value of  $0.0 m^3/kg$  indicates all contaminant remains in the aqueous phase with no adsorption to surrounding medium, and a  $K_d$  value greater than  $0.0 m^3/kg$  allows for adsorption on to the solid medium. Subsequently, a COPC with a  $K_d$  of  $0.0 m^3/kg$  will be transported more quickly. A fabricated radionuclide GenRad, with a  $K_d$  of  $0.0 m^3/kg$  and large half-life was chosen for this sensitivity analysis. Artificial values for  $K_d$ , ranging from 0.0005 to  $5.0 m^3/kg$ , were assigned to GenRad and mass release curves generated on plots show the effect on transport. GenRad has an assigned half-life of  $1E+50$  years, which eliminates radioactive decay from contributing to the sensitivity analysis results. Figure 21 below shows that GenRad with a  $K_d$  of less than  $0.0005 m^3/kg$  will be completely released from the grouted waste monolith in less than 500 years. A  $K_d$  value of  $0.05 m^3/kg$  still has 55% of the mass remaining in the monolith at 3,000 years.

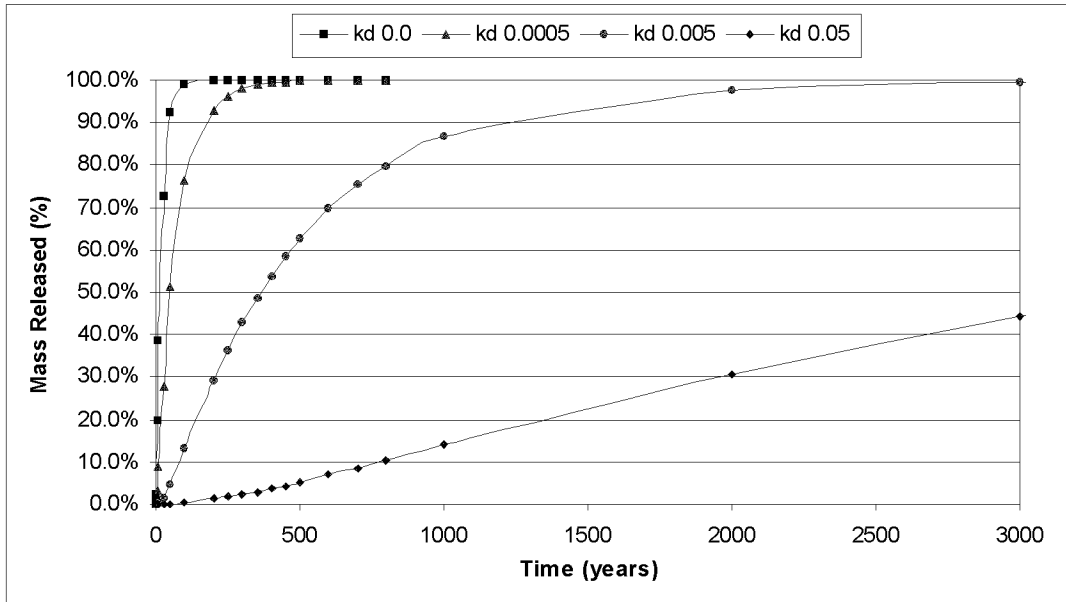


Figure 21. Mass release of GenRad with  $K_d$  values of 0.0, 0.0005, 0.005 and 0.05  $\text{m}^3/\text{kg}$  during 3,000 years.

Mass release curves for  $K_d$  values of 0.05, 0.5, and 1.0  $\text{m}^3/\text{kg}$  are shown in Figure 22. In this figure, the abscissa has been extended to 20,000 years to show how increasing the  $K_d$  lengthens the time of release. The mass release curve for a  $K_d$  0.05  $\text{m}^3/\text{kg}$  shows that 98% has been released from the monolith after 20,000 years.  $K_d$  values greater than 0.5  $\text{m}^3/\text{kg}$  indicate the release from the monolith is not in excess of 30% of the initial mass over this period.

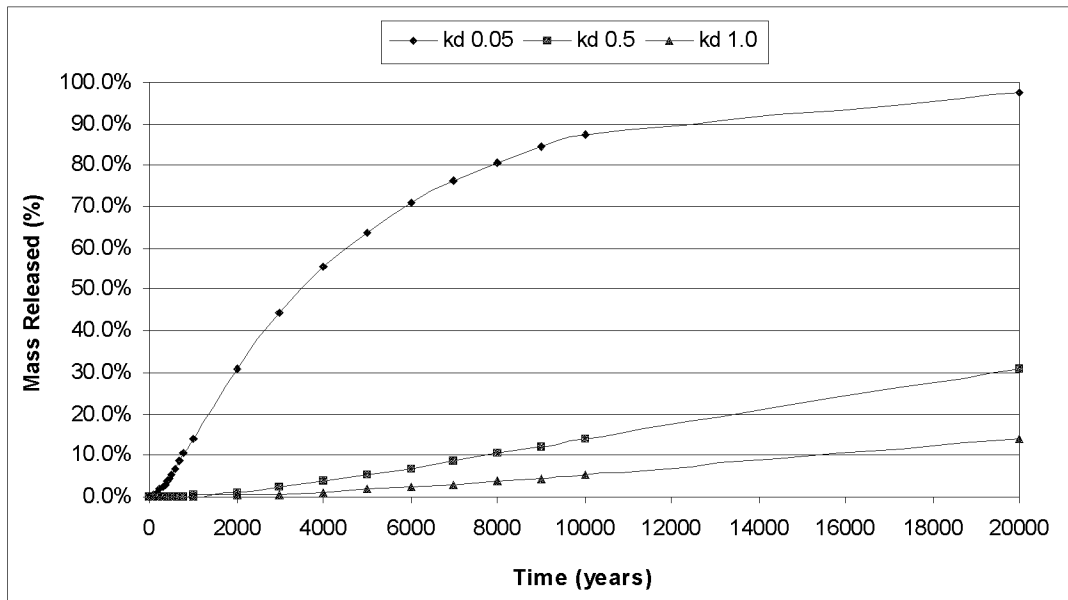


Figure 22. Mass release of GenRad with  $K_d$  values of 0.05, 0.5 and 1.0  $\text{m}^3/\text{kg}$  during 20,000 years.

Figure 23 indicates  $K_d$  values greater than  $1.0 \text{ m}^3/\text{kg}$  will release less than 5.3% of the initial mass of GenRad during 10,000 years. Extending the time to 20,000 years indicates a mass release of less than 5.3% and 1.2% for  $K_d$  values of 2.0 and  $5.0 \text{ m}^3/\text{kg}$ .

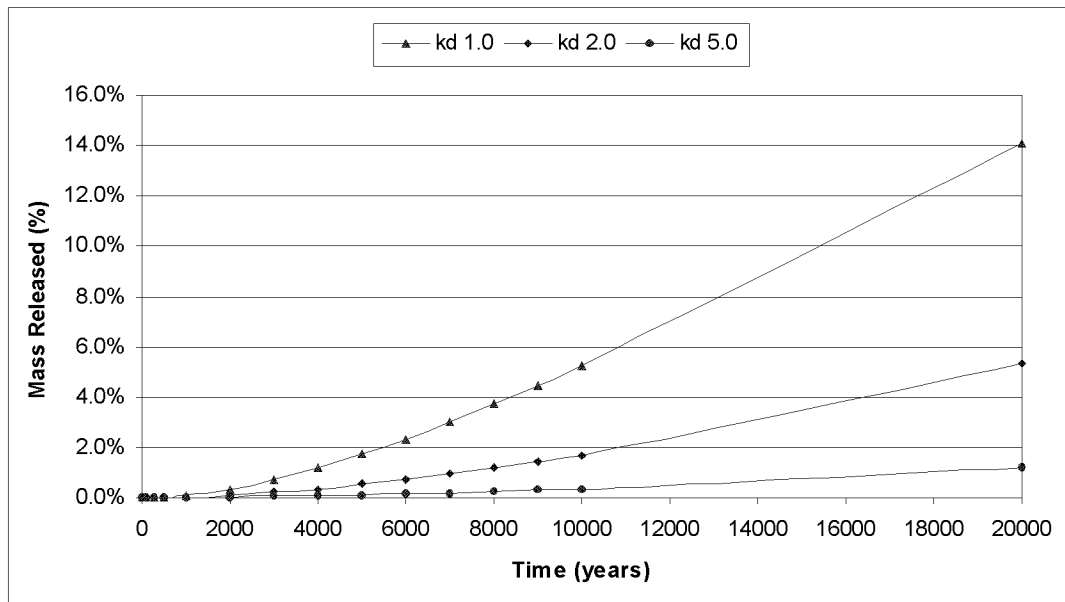


Figure 23. Mass release of GenRad with  $K_d$  values of 1.0, 2.0, and  $5.0 \text{ m}^3/\text{kg}$  during 20,000 years.

The sensitivity analysis of the distribution coefficient indicates that radionuclides with  $K_d$  values less than  $0.005 \text{ m}^3/\text{kg}$  will be released within 3,000 years. Compounds with  $K_d$  values less than  $0.05 \text{ m}^3/\text{kg}$ , will be 90% released in more than 10,000 years.  $K_d$  values greater than  $0.05 \text{ m}^3/\text{kg}$  are expected to retain 70% of the COPC within the monolith. The greatest effect on contaminant release occurs when the  $K_d$  values changes from 0.05 to  $0.5 \text{ m}^3/\text{kg}$ . The release of radionuclides with  $K_d$  values greater than  $1.0 \text{ m}^3/\text{kg}$  is very slow; with less than 5.3% of the initial mass released in 10,000 years.

**3.10.2.4 Sensitivity to Radioactive Decay.** The half-life of a radionuclide can contribute a significant amount to mass loss of COPC from the monolith. Mass loss is a combination of loss through hydraulic transport ( $K_d$  related) and the loss through depletion caused by radioactive decay. If the  $K_d$  is large enough to restrict transport of the radionuclide, the half-life, depending on how small the value is, can have a significant effect on the loss of mass over time. The intrinsic interaction between physical transport and radioactive decay in contributing to radionuclide release is generalized in Tables 25 and 26. The tables provide a way to determine the approximate amount of radionuclide mass released from the monolith over time, by combining the distribution coefficient of the grout and element with the half-life of that element. Table 25 shows how much mass is released at the 1,000-year mark and Table 22 shows release at 10,000 years.

Table 25. Mass release of contaminants of potential concern from monolith at 1,000 years according to  $K_d$  and half-life.

Half-Life (yrs)	1,000 yrs				Distribution Coefficient $K_d$		
	0.0005	0.005	0.05	0.5	1	2	5
100	100.00%	99.92%	99.69%	99.66%	99.66%	99.66%	99.66%
500	100.00%	95.79%	76.67%	73.44%	73.39%	73.37%	73.36%
1,000	100.00%	92.59%	55.86%	49.33%	49.22%	49.19%	49.17%
5,000	100.00%	88.18%	24.93%	13.18%	12.97%	12.91%	12.89%
10,000	100.00%	87.45%	19.67%	7.00%	6.78%	6.71%	6.69%
50,000	100.00%	86.84%	15.17%	1.71%	1.48%	1.41%	1.38%
100,000	100.00%	86.76%	14.59%	1.03%	0.79%	0.72%	0.70%
500,000	100.00%	86.69%	14.12%	0.48%	0.24%	0.17%	0.15%
1,000,000	100.00%	86.69%	14.07%	0.41%	0.17%	0.10%	0.08%
10,000,000	100.00%	86.68%	14.01%	0.35%	0.11%	0.04%	0.02%

For example, the radioactive element Nb-94 has a half-life of 20,000 years and a  $K_d$  of 1.0 m<sup>3</sup>/kg for grout. Table 21 shows that approximately less than 6.78% of the compound would be released at 1,000 years. At 10,000 years, the amount released would be closer to and less than 51.58% of the initial mass present (see Table 26).

This comparison illustrates that as  $K_d$  increases and retards radionuclide transport, the amount of mass lost or released is attributed to depletion through radioactive decay.

The presence of fractures is another important physical parameter influencing the release of contaminant from the monolith. Fracture sensitivity analysis was performed for a range of fractures extending vertically in the x-y planes. GenRad was used in the fracture analysis (no  $K_d$  or half-life). Figure 24 compares the mass release of GenRad of a nonfracture condition with an increasing presence of fractures.

Table 26. Mass release of contaminants of potential concern at 10,000 years according to  $K_d$  and half-life.

Half-Life (yrs)	10,000 yrs				Distribution Coefficient $K_d$		
	0.0005	0.005	0.05	0.5	1	2	5
100	100.00%	100.00%	100.00%	100.00%	100.00%	100.00%	100.00%
500	100.00%	100.00%	100.00%	99.99%	99.99%	99.99%	99.99%
1000	100.00%	100.00%	99.91%	99.67%	99.65%	99.64%	99.64%
5000	100.00%	100.00%	95.97%	76.56%	74.45%	73.63%	73.33%
10000	100.00%	100.00%	92.98%	55.82%	51.58%	49.90%	49.27%
50000	100.00%	100.00%	88.87%	24.99%	17.39%	14.34%	13.18%
100000	100.00%	100.00%	88.19%	19.73%	11.54%	8.25%	7.00%
500000	100.00%	100.00%	87.63%	15.25%	6.55%	3.05%	1.72%
1000000	100.00%	100.00%	87.55%	14.67%	5.91%	2.38%	1.03%
10000000	100.00%	100.00%	87.49%	14.14%	5.32%	1.77%	0.41%

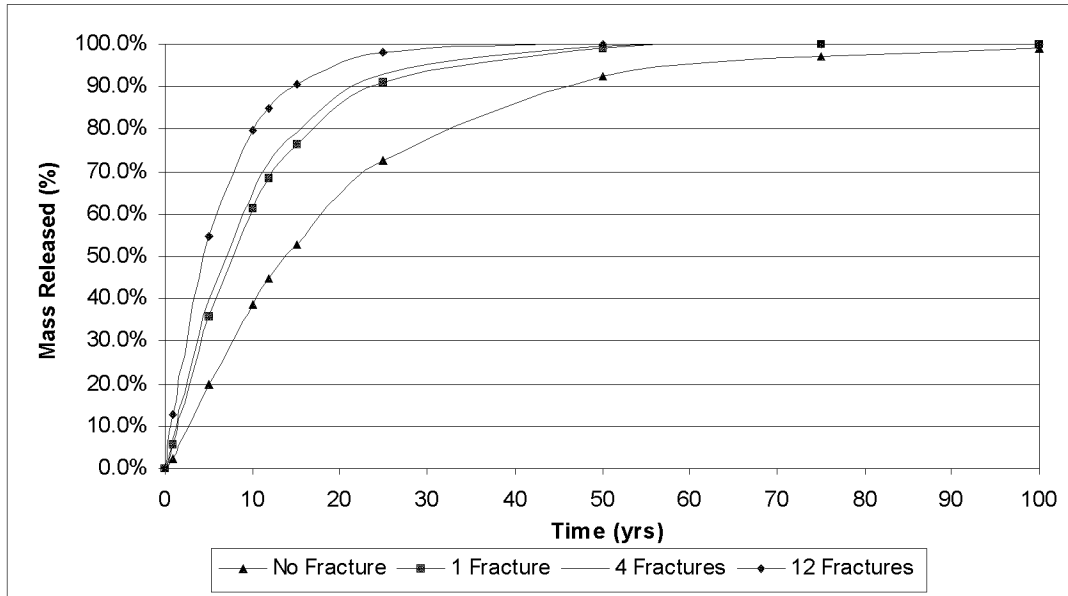


Figure 24. Mass release of GenRad from nonfractured to fractured condition of the monolith.

Introducing a single fracture into the monolith shows a significant increase in the amount of mass of GenRad released, compared to a nonfractured condition. The time for complete release from the monolith is approximately 50 years, or half the time required for release from a nonfractured condition. As the number of fractures increases, so does the amount of mass released. The time for complete release decreases. Table 27 below shows the difference in the fracture volume and the interface area of the fractures within the matrix.

Table 27. Comparison of fracture volume and permeability.

Fractures	Fracture volume (m <sup>3</sup> )	Fracture Interface Area (m <sup>2</sup> )
1	0.000852	8.52
4	0.003408	34.08
12	0.010224	102.48

Table 28 provides the percentage difference in the amount of mass released over 100 years. As shown, the presence of a single fracture immediately increases the mass released from the monolith. However, any further increase in the number of fractures after 12 showed little increase in the release of mass. From the analysis it was determined that any further increase in the number of fractures beyond 96 did not increase the amount of mass released, nor the time for complete release from the monolith, therefore indicating that 96 is the threshold fracture number for maximum release of contaminant.

### 3.10.3 Sensitivity Case Analysis Summary

In summary, the sensitivity analysis of model discretization has shown that increasing resolution of the mesh reduces the moisture content retained over 10,000 years. With less water retained, more water flows through the monolith, thereby increasing the amount of mass of COPC released. This is supported in Figures 18 and 19. However, the time for complete release of mass from the monolith remained unaffected, considering the 10,000 years by which the simulation is bounded.

Table 28. Percentage of mass released (GenRad) as the presence of fractures increases in the monolith.

Years	No Fracture	1	4	12	24	48	96	200
0	0.00%	0.00%	0.00%	0.00%	0.00%	0.00%	0.00%	0.00%
1	2.22%	5.67%	7.88%	14.96%	15.80%	15.94%	15.91%	15.88%
5	20.00%	36.90%	40.83%	57.00%	59.11%	59.85%	60.02%	58.81%
10	38.56%	63.31%	66.88%	81.42%	80.89%	82.59%	83.37%	83.27%
12	44.93%	70.45%	73.75%	86.90%	87.25%	87.71%	88.27%	88.19%
15	53.06%	78.73%	81.40%	92.17%	92.66%	92.43%	92.79%	92.74%
25	72.55%	92.64%	94.06%	98.51%	98.72%	98.59%	98.66%	98.65%
50	92.26%	99.49%	99.65%	99.98%	99.98%	99.97%	99.97%	99.97%
75	97.32%	100.00%	100.00%	100.00%	100.00%	100.00%	100.00%	100.00%

Parameter sensitivity analysis revealed that infiltration and intrinsic permeability had little effect on mass release from the monolith. The parameter having the greatest effect on mass release was fractures present within the grouted monolith. A baseline fracture density of 6.25 fractures per planar area indicated that compounds with a zero  $K_d$  are released in a quarter of the time it takes the same compound to escape a nonfractured medium. This result needs a more thorough investigation, incorporating fractures into the model design and operation. Finally, the sensitivity analysis revealed where investigation is needed to determine the adsorptive characteristics of COPCs with various immobilizing agents. Figure 25 indicates how effective the distribution coefficient is in retarding contaminant transport. The time for complete release in Figure 25 is approximately 100 years. The amount released declines as the distribution coefficient increases, in successive orders of magnitude starting with 0.0005 m<sup>3</sup>/kg. Results from the  $K_d$  sensitivity analysis indicated that COPCs with  $K_d$  equal to and greater than 0.5 m<sup>3</sup>/kg would have 70% of the mass retained during 10,000 years of immobilization. This is an important result considering that compounds like uranium and plutonium have  $K_d$  for grout of 1.0 and 5.0 m<sup>3</sup>/kg, respectively.

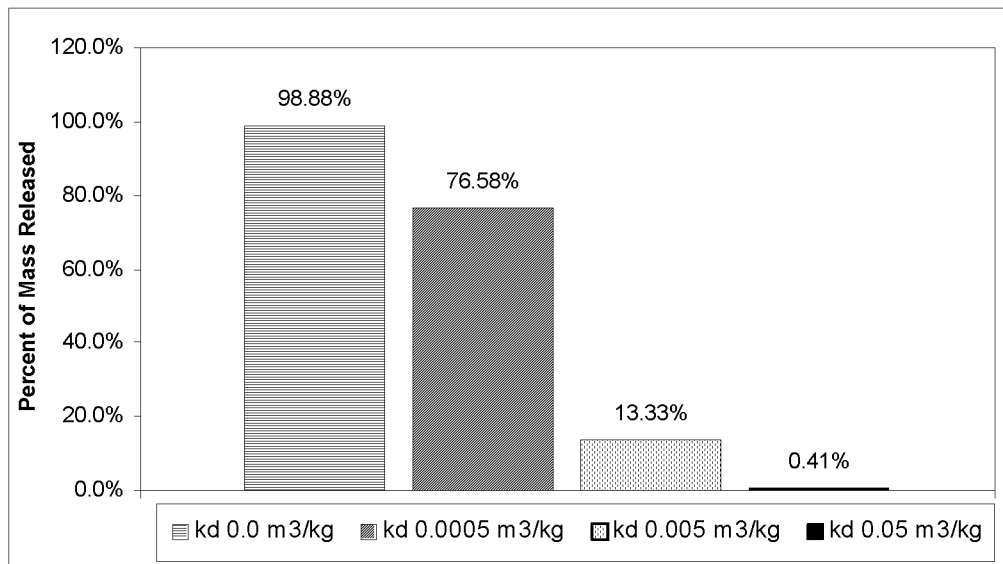


Figure 25. Mass release from monolith as the  $K_d$  increases in magnitude in 100 years.

## **3.11 Modeling Limitations**

TOUGH2 has many capabilities and is suited for modeling multiple phase, multiple dimensions (1D, 2D and 3D), and radioactive decay; however, the scope of this project exceeded the functionality of the code. Specifically, TOUGH2 cannot explicitly model chemical solubility. Chemical solubilities are not coded within the architecture of TOUGH2. Unfortunately, many of the COPCs are in quantities that exceed the aqueous phase limit and TOUGH2 is unable to accurately model phase equilibriums under that condition.

### **3.11.1 Modeling Uncertainties**

Another limitation of the code is the lack for modeling geochemical interactions between the medium and the fluid. Incorporating geochemical interactions like self-annealing and disintegration has important affects for estimating mass release over the life span of the monolith. The integrity of the monolith is of extreme importance as seen from the sensitivity analysis involving the presence of fractures.

By modeling this project in a 3D configuration, dispersive affects were not considered. Considering the length of simulation, 10,000 years, dispersion of contaminants would influence lateral spreading as well as contribute to mass release via vertical transport. This added parameter to transport would increase the estimated time for contaminant release. The extent to which contaminants would possibly spread would be valuable information in assessing the effectiveness of grout injection.

### **3.11.2 Modeling Limitations**

The lack of calibration for this model design is perhaps the greatest limitation to the project and creates uncertainty. It is impossible to draw conclusive results on the accuracy and reliability of results because of the lack of data surrounding radionuclide release from material such as grout, that has parameters as described in this report.